Lithos 318–319 (2018) 267–282

Contents lists available at ScienceDirect

Lithos

journal homepage: www.elsevier.com/locate/lithos

Decoding a post-collisional multistage magma system: The Quaternary ignimbrites of Aragats stratovolcano, western Armenia

Hripsime Gevorgyan [a,b,*], Alexander Repstock [b], Bernhard Schulz [c], Khachatur Meliksetian [a], Christoph Breitkreuz [b], Arsen Israyelyan [a]

[a] Institute of Geological Sciences, National Academy of Sciences of Armenia, Marshal Baghramyan Avenue, 0019 Yerevan, Armenia
[b] Institute for Geology, TU Bergakademie Freiberg, Bernhard-von-Cotta Straße 2, 09599 Freiberg, Saxony, Germany
[c] Institute for Mineralogy, TU Bergakademie Freiberg, Brennhausgasse 14, 09596 Freiberg, Saxony, Germany

ARTICLE INFO

Article history:
Received 28 February 2018
Accepted 20 July 2018
Available online 26 July 2018

Keywords:
Aragats
Ignimbrite
Glass chemistry
Mineral texture
Magma mingling
Mixing
Geothermobarometry

ABSTRACT

Quaternary eruptions from an intraplate multistage magma reservoir of the Aragats stratovolcano in western Armenia formed pyroclastic density currents and fallouts deposited in an area around 2,000 km^2, comprising six ignimbrite units and three fallout deposits. Published K/Ar and Ar/Ar age data allow for a distinction between older (Calabrian, 1.8–0.90 Ma) and younger (Middle Pleistocene, 0.75–0.65 Ma) ignimbrites. The detailed characterization of the crystal-poor to crystal-rich, trachyandesitic to rhyolitic ignimbrite sequence deciphers the pre-eruptive magmatic conditions. It also contributes to the understanding of Plinian eruptions of the largest volcanic complex in the Lesser Caucasus.

The chemical variation of pumice fragments reveals the conditions of both, homogeneous and mingled heterogeneous magma systems. The phenocryst assemblage of the older crystal-poor units (Ab-rich plagioclase + amphibole ± pyroxene) indicates growth in a cooler hydrous magma chamber, whereas the partially resorbed phenocrysts of the younger crystal-rich units (An- to Ab-rich plagioclase + pyroxene) suggest growth in a superheated magma chamber fueled by mafic, mantle-derived melts. In the younger units, external (e.g. sieve fabrics) and internal phenocryst textures have been generated by decompression and convection during ascent. With the older units, the chemical variation in amphibole from core to the narrow break-down rim reveals magma ascent from a deep (13 km depth) to a shallow (up to 8 km) level.

Tracking the p-T paths of cumulate fragments (pyroxene, plagioclase) in the younger units, we estimate the depth of the anhydrous crystal-rich magmatic chamber at around 25 km. Based on the composition of clinopyroxene cumulates, we propose a multi-stage evolution of melts from subalkaline and tholeiitic to calc-alkaline composition. The pronounced high Zr content and Zr/Hf ratios of the entire Upper Pliocene to Quaternary post-collisional magmatism could be attributed to partial melting of an enriched mantle source in the Lesser Caucasus.

1. Introduction

The Quaternary Aragats stratovolcano in western Armenia forms the highest peak in the Lesser Caucasus (4,090 m) and it is one of the largest volcanic centers (base diameter: 40–42 km) in the Turkish-Armenian-Iranian Plateau (e.g. Meliksetian, 2012). It comprises large ignimbrite units and lava flows covering an area >5,000 km^2 (Fig. 1; Jrbashyan et al., 2012). The Aragats Volcanic Province (AVP) ignimbrites and associated fallout deposits mark an important explosive component of the evolution of the Aragats stratovolcano which is otherwise dominated by lava flow activity. The largest pyroclastic flow sheet has a volume of at least 5 km^3 (VEI ≥ *5;* Gevorgyan, 2013).

The pyroclastic deposits of this stratovolcano contain crystal-poor (up to 25 vol.-%; Shirinyan, 1961) and crystal-rich units (up to 40 vol.-%; Gevorgyan, 2013). Silica-rich crystal-poor ignimbrites of intra-continental settings often comprise a "dry" mineral assemblage, such as pyroxene, and show a lack of evolved silicates like quartz and sanidine (Bachmann and Huber, 2016; Ellis et al., 2014). Ellis et al. (2014) investigated cumulate fragments of the intra-continental "dry" Snake River Plain volcanic rocks (Idaho, USA) and suggested eruption from a multi-batch magma system. However, crystal-poor ignimbrites such as the Rahopaka ignimbrites in Matahana Basin (New Zealand; Ritchie, 1996) can also comprise hydrous mineral assemblages and originate from H_2O-rich zoned magma chambers. These systems are

* Corresponding author at: Institute of Geological Sciences, National Academy of Sciences of Armenia, Marshal Baghramyan Avenue, 0019 Yerevan, Armenia.
E-mail address: hripsime.gevorgyan@geology.am (H. Gevorgyan).

https://doi.org/10.1016/j.lithos.2018.07.024
0024-4937/

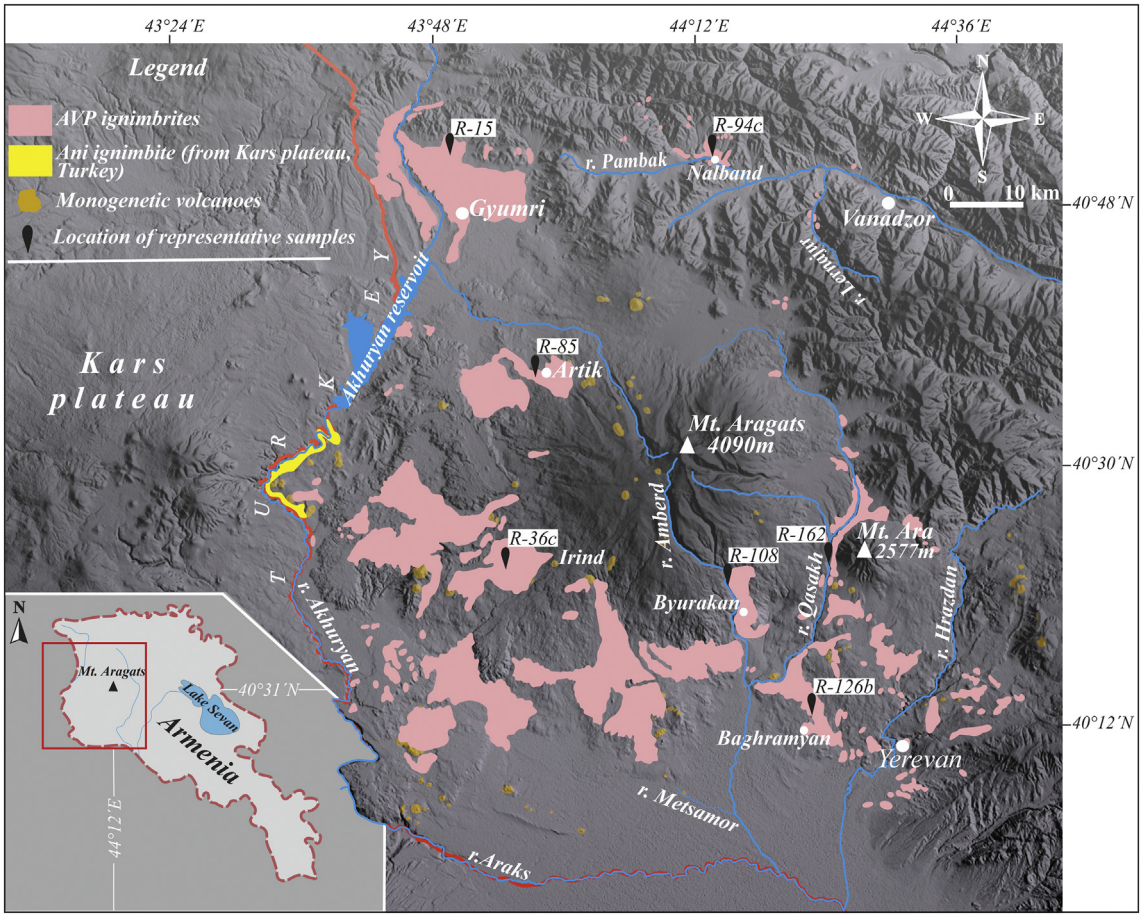

Fig. 1. Digital elevation map of the Aragats Volcanic Province, western Armenia, depicting the outcrop areas of ignimbrite sheets (modified after Shirinyan, 1961; Ghukasyan, 1985). The Ani ignimbrite exposed in the westernmost part of AVP is presumably originated from Aladja volcano in the eastern part of Kars plateau in Turkey (Karapetyan, 1992) and it is not related to Aragats volcano.

known to be saturated with volatiles insufficient to unlock the mush for eruption (Huber et al., 2012). Other representatives of zoned ignimbrites are known from the Nelson Mountain and the Carpenter Ridge Tuffs (Colorado, USA), where silica-rich crystal-poor magmas graded into hotter crystal-rich intermediate magmas. This results in gradually zoned pyroclastic deposits (e.g. Bachmann and Huber, 2016; Hildreth, 1981). Crystal-rich ignimbrites from super eruptions, such as Fish Canyon and Cebolla Creek Tuffs (Colorado, USA), represent remobilized and partially molten portions of a cumulate mush (Bachmann and Huber, 2016; Huber et al., 2012). Remobilization is controlled by injection of fresh mafic magmas (Bachmann and Huber, 2016; Huber et al., 2012; Smith, 1979).

The pre-eruption dynamics of the magma reservoir can be traced by textural and chemical analysis of phenocrysts. Information of these processes are preserved in external anhedral resorption, dusty or sieve textures (e.g. Renjith, 2014; Tsuchiyama, 1985) and internal textures such as reverse, normal and oscillatory zoning (e.g. Crabtree and Lange, 2011; Ginibre et al., 2007). The external textures clearly indicate disequilibrium of the crystal with the melt, caused by injections of mafic magma (e.g. Steward and Pearce, 2004), whereas internal textures can track mixing or compositional fluctuation in the melt (e.g. Crabtree and Lange, 2011). Partial to complete breakdown of hydrous minerals, such as amphibole, is an indicator for single- or multi-stage magma ascent (Browne and Gardner, 2006; Rutherford and Hill, 1993). Moreover, the chemical composition of phenocrysts and glass shards can be used as geothermo- and barometers, which give information about crystallization conditions in the magma reservoir (e.g. Putirka, 2008). Within neighboring volcanic complexes in eastern Anatolia, several applied barometers showed depths of magma chambers at ca. 15 km (e.g. Süphan and Nemrut volcanoes; Özdemir et al., 2011; Peretyazhko et al., 2015).

Most of the previous studies on the pyroclastic units and lava flows of the AVP focused on petrography and lithostratigraphy (e.g. Ghukasyan, 1985; Karapetyan, 1992; Shirinyan, 1961). Several geochemical studies on lava complexes have been carried out (Djerbashyan, 2010; Ghukasyan, 1983; Meliksetian, 2012). Applying new geochemical data on whole rock, fiamme, glass shards and minerals we attempt to re-evaluate the lithostratigraphy, understand the mechanisms that led to the eruption of crystal-poor and crystal-rich melts and to shed light on the magmatic evolution and tectonic setting for one of the largest volcanoes in the Arabia-Eurasia collision zone.

2. Geological setting and previous studies

The territory of Armenia forms part of the northern sector of the Turkish-Iranian Plateau, the geodynamics of which are the result of the continental collision between the Eurasian and the Arabian plates. Neogene and Quaternary volcanism and seismic activity in the region are considered to reflect this plate interaction (e.g. Jrbashyan et al., 2012; Karakhanyan et al., 2013; Koçyiğit et al., 2001). Neill et al. (2015) supposed that the Late Cenozoic collisional magmatism within the Turkish-Iranian Plateau, including the Armenian sector, may be

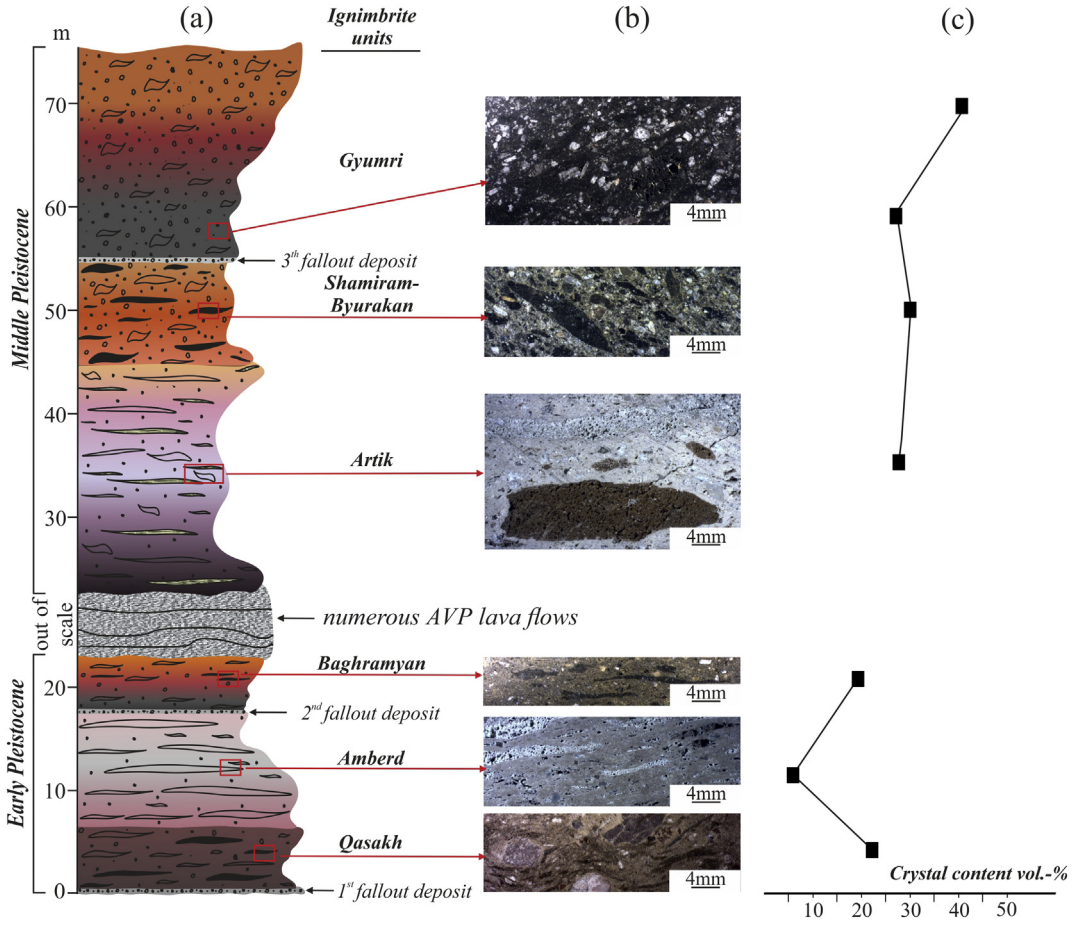

Fig. 2. a) Generalized lithological column of AVP ignimbrites and associated fallout deposits: In places, ignimbrites of Qasakh and Amberd canyons are overlain by numerous basaltic trachyandesitic lava flows. b) Photos of rock slabs of AVP ignimbrites. c) Phenocryst content (vol.-%) diagram.

conditioned by mantle dynamics like asthenospheric upwelling, which in turn initiated partial melting of lithospheric mantle.

The AVP, which covers an area of >5,000 km^2, stands out for its size and the abundance and variety of pyroclastic deposits (ignimbrites and fallout deposits, Jrbashyan et al., 2012). The basement of AVP comprises Proterozoic metamorphic rocks, Mesozoic to Paleogene folded complexes as well as Neogene sedimentary and volcanic units. The geothermal gradient for Aragats stratovolcano is around 5.5 °C per 100 m (Badalyan, 2000). The Aragats stratovolcano and the surrounding volcanic plains host >93 monogenetic scoria cones and lava domes (IAEA-TECDOC-1795, 2016). Another polygenetic complex, Arailer volcano, is located at the eastern margin of AVP (Fig. 1). In the plains around Aragats volcano, the pyroclastic succession typically has a mean thickness of 75 m, however, in some deeply incised canyons, like Amberd (Fig. 1), lava and pyroclastic sheets may accumulate >600 m.

The sequence of AVP ignimbrites and its petrographic features have been described somewhat controversially (e.g. Ghukasyan, 1985; Karapetyan, 1992; Shirinyan, 1961). Shirinyan (1961) subdivided the AVP ignimbrites into four main units, from base to top: 1) ignimbrites of Amberd and Qasakh canyons, 2) first unit of Yerevan-Leninakan ignimbrite, 3) Artik "tuffo-lava", and 4) second unit of Yerevan-Leninakan ignimbrite. For the latter, this author separated another subunit, the fiamme-rich Shamiram-Byurakan ignimbrite. Here, we adopt the general stratigraphic scheme proposed by Shirinyan (1961) and Ghukasyan (1985), with the following modifications: (i) Shirinyan (1961) and Ghukasyan (1985) considered the Amberd and Qasakh ignimbrites to represent one single unit, and Shamiram-Byurakan ignimbrite as a subunit of the Gyumri ignimbrite. However, we separate these ignimbrite units based on field relationships and petrological characteristics. (ii) Shirinyan (1961) named two ignimbrite units of different age as "first and second units of Yerevan-Leninakan ignimbrite" based on their similar color range; in order to reduce confusion, we rename these pyroclastic flow deposits as Baghramyan and Gyumri ignimbrites, respectively (Fig. 2).

The volcanic activity of Aragats began in the Early Pleistocene and continued up to the Middle Pleistocene, and it consists of four main stages (Ghukasyan, 1985). By K/Ar ages, the Amberd ignimbrite corresponds to 1.8 Ma[1] (Ghukasyan, 1985). Based on the field observations and correlations of the widely separated outcrops in AVP, the approximate age of the Artik ignimbrite, which by stratigraphic position lies between a dacitic lava flow of the third activity stage of Aragats volcano and the Gyumri ignimbrite, should be in the range of 0.72 Ma and 0.65 Ma. Mitchell and Westaway (1999) published a K/Ar age of 0.90 ± 0.08 Ma for an ignimbrite unit near Nalband village (sampled as 3B2), which we consider as the equivalent of Baghramyan ignimbrite (see below). Another unit at the same locality (sampled as 3B3), which we correlate with Gyumri ignimbrite, yielded an age of 0.75 ± 0.06 Ma. $^{40}Ar/^{39}Ar$ age determination of fiamme and plagioclase yielded 0.65 ± 0.04 Ma and for 0.66 ± 0.04 Ma for the Gyumri and Shamiram-Byurakan ignimbrites, respectively (IAEA-TECDOC-1795, 2016). These ages are consistent with earlier K/Ar age determinations of under- and overlying lava flows (Chernyshev et al., 2002) and with paleontological data on rodents (Melik-Adamyan, 1994). The youngest AVP volcanic rocks comprise trachybasaltic-andesite lava complexes

[1] No error range given in the publication.

(0.53 ± 0.07 Ma and 0.45 ± 0.07 Ma, Chernyshev et al., 2002) and trachydacites of Irind volcano, (Fig. 1; 0.49 ± 0.03 Ma, IAEA-TECDOC-1795, 2016), overlying Gyumri and Shamiram-Byurakan ignimbrites.

It is worth stressing that several geothermometers were applied by Ghukasyan (1983), each based on different crystal-crystal (two pyroxenes, orthopyroxene-olivine) or crystal-liquid (olivine-liquid) equilibria showing that AVP mafic magmas had temperatures in the range 1100–1250 °C and the reservoir was in 30 to 40 km depth. Whereas, based on experimental studies, Djerbashyan (2010) estimated crystallization temperatures of basalts in the range of 1120-1175 °C and of andesites at 1141-1159 °C, under pressures of 4.6 to 4.8 kbar and 4.4 to 4.5 kbar, respectively.

3. Methods

A total of 175 pyroclastic samples were collected from >62 exposures around the Aragats stratovolcano. The chemical composition of twelve representative ignimbrite whole rock samples, six samples of ash and lapilli separated from fallout deposits and eight pumice fragments from ignimbrites was analyzed at ALS Minerals in Dublin (Ireland; data and standards are presented in Table A1). Major oxides and base metals have been analyzed with the ICP-AES, trace and rare earth elements by the ICP-MS method.

We included geochemical analyses (62 ignimbrite whole rock samples, five samples from ash- and lapilli layers, and of 16 fiamme samples) determined by atomic absorption spectro-photometry (AAS-photometry), gravimetric, photocolometric, titrimetric and flame photometric carried out at the Institute of Geological Science, National Academy of Science of Armenia (data and standards in Table A2).

Preliminary qualitative compositional analyses (EDS) and back-scattered electron images were performed by FEI QUANTA 600F and 650F scanning electron microscopes at the Institute for Mineralogy, TU Bergakademie Freiberg (Germany).

The chemical composition of phenocrysts and glass shards from seven representative thin sections of AVP ignimbrites was examined with a JEOL JXA-8900RL electron microprobe analyzer at the Institute for Material Science, TU Bergakademie Freiberg (Germany; Tables A3 to A7). Operating conditions were performed with an accelerating voltage of 15 kV and probe current at 20 nA with a beam diameter of up to 2 μm (Na was measured first and a ZAF correction has been applied, standards in Table A4).

4. Results

4.1. Lithostratigraphy and petrography

The pyroclastic succession of AVP starts with a well-sorted, clast-supported pinkish ash layer (≤ 0.5 m in thickness; "1st Plinian fallout deposit", Fig. 2). It is covered by a ≤ 1.5 m thick unit of Qasakh ignimbrite (~23 vol.-% phenocrysts), well-exposed in outcrops along the canyons of Qasakh and Amberd rivers (eastern and southeastern part of AVP; Fig. 2). In contrast, the overlying crystal-poor Amberd ignimbrite (up to 11 m thick, ~8 vol.-% of phenocrysts; Fig. 2) solely outcrops at Amberd canyon. A sharp contact between these two pyroclastic units (Qasakh and Amberd) can be observed in the Amberd canyon close to Aghtsq village. The grey-pinkish, strongly flattened fiamme of the Amberd ignimbrite displays parataxitic texture with spherulitic crystallization, whereas the fiamme of the Qasakh unit shows dark pink-reddish color and a glassy vesicular texture. Locally, these units are covered by lava flows of trachybasaltic to (trachy-)dacitic composition (Ghukasyan, 1985), and they are in turn covered by the Gyumri ignimbrite.

The occurrence of Baghramyan ignimbrite is restricted to the southern and southeastern peripheries of the AVP and several small outcrops are located north of the AVP along the Pambak valley (Fig. 1). Here, this unit is underlain, in places, by a well-sorted, clast-supported grey to black fallout ash layer (≤0.2 m in thickness; "2nd Plinian fallout deposit", Fig. 2a). The crystal-poor Baghramyan ignimbrite is slightly to moderately welded and is showing black to reddish colors. The amount of flattened fiamme decreases towards the top. In the Arich gorge (northwestern part of AVP, Fig. 1) Baghramyan ignimbrite is overlain by the Artik ignimbrite, whereas at Baghramyan (southwestern part of AVP) and at Nalband (northern AVP) villages this unit is covered by Gyumri ignimbrite (Fig. 2a, b).

The Artik ignimbrite is widely distributed in the northern and northwestern part of AVP and it can also be observed in the northeastern slopes and foothills of the Aragats massif with a maximum thickness of 28 m (Fig. 2a, b). Within the unit, we distinguish two different types of pumice fragments, termed here as α- and β-fiamme. The dark pink-reddish α-fiamme have a glassy vesicular texture and it hosts euhedral and subhedral phenocrysts of plagioclase, pyroxene, and Fe—Ti oxides. More abundantly, the light grey colored, strongly flattened β-fiamme reveal spherulites, comprising tridymite and cristobalite.

In contradiction to the observations of Shirinyan (1961), a distinct contact and, in some exposures, a smooth transition between the Artik and Shamiram-Byurakan ignimbrites can be seen near Antarut village and on the top of several scoria cones of Shamiram plateau. This information demonstrates that the Shamiram-Byurakan ignimbrite was erupted after Artik ignimbrite and cannot be a subunit of the younger Gyumri ignimbrite (Fig. 2a, b). In the Shamiram-Byurakan ignimbrite, two types of fiamme were observed: 1) light brownish vesicular-vitric and 2) black dense obsidian-like.

The base of the 15 m thick crystal-rich (~40 vol.-%) Gyumri ignimbrite is underlain by a dark grey-blackish, well-sorted and clast-supported ash layer, the "3rd Plinian fallout deposit" (≤0.4 m in thickness, Fig. 2a-c). By areal extension, this fallout deposit together with Gyumri ignimbrite is the most widespread pyroclastic unit around Aragats and it is well exposed, particularly in quarries in the western part of AVP. In comparison with above-mentioned AVP ignimbrites, Gyumri unit is generally poor in pumice (up to 2 cm in length) and it reveals vesicular texture and variable degrees of welding.

The Pambak ignimbrite (Fig. 2a, b), second ignimbrite unit exposed along the Pambak and Lernajur rivers (52 km north of Aragats peak, Fig. 1), has been considered as a product of a local fissure eruption not belonging to AVP (Ghukasyan, 1985). However, following Karapetyan (1992), we consider it to be a distal equivalent of Gyumri ignimbrite. This assertion is supported by similar crystal and pumice fragment content of Pambak and Gyumri ignimbrites. Also, both display similar vesicular fiamme with ≤2 cm in length.

Two different phenocryst assemblages were observed in AVP ignimbrites: (1) the crystal-poor Qasakh, Amberd and Baghramyan units are dominated by An-poor plagioclase and OH-rich ferromagnesian crystals such as magnesiohastingsite, edenitic hornblende, and (2) the crystal-rich Artik, Shamiram-Byurakan and Gyumri (with Pambak stratigraphically equivalent) units are dominated by An-rich plagioclase and "dry" mafic mineral assemblages (augite, diopside and enstatite-ferrosilite solid solution). The crystalline groundmass of the AVP ignimbrites is composed of the same phases as the phenocrysts.

4.2. Whole rock and glass geochemistry

The majority of the investigated samples from AVP ignimbrites and associated fallout deposits show (trachy-)andesitic and trachytic composition, plotting below the transition line between alkaline and subalkaline series (Fig. 3a). Following the classification of Peccerillo and Taylor (1976), the AVP pyroclastic products exhibit high-K calc-alkaline character and mostly consist of high-K andesite to dacite, whereas the Amberd ignimbrite shows range in composition from high-K dacite to rhyolite (Tables A1 and A2). The normative mineralogy exhibits a wide range of normative quartz content in the AVP pyroclastic sheets. Mainly in the younger AVP pyroclastic sheets, it ranges from 7.6 to 19.6 wt.-% (Table A2). Nevertheless, the 1st fallout deposit and

the Amberd ignimbrite show higher normative quartz content (up to 20.9 and 28.2 wt.-%, respectively; Table A2) rendering them of (trachy-)dacitic and rhyolitic composition. This contradicts to the observations of Shirinyan (1961), who argued the pyroclastic rocks showed an andesitic to (trachy-)dacitic trend.

Almost all the AVP pyroclastic units are silica-saturated. The lowest amount in SiO_2-content with 56.9 wt.-% can be reported for the trachyandesitic, the uppermost part of the Gyumri ignimbrite (Fig. 3a). The SiO_2 content of groundmass glass-shards of the older ignimbrite units ranges from 64.8 to 72.6 wt.-% (EMPA; Table A3) reflecting a chemical variability of subalkaline rhyolitic and highly alkaline trachytic composition ($Na_2O + K_2O$ = 6.8–12.3 wt.-%; Fig. 3a; Table A3). Compared to the whole-rock composition of the older AVP units (SiO_2 = 62.3–70.4 wt.-%; $Na_2O + K_2O$ = 7.1–9.8 wt.-%; Tables A1 and A2), the glass shards revealed higher values. In the same way, for the younger AVP ignimbrite units, a high silicic trend was detected (Fig. 3a). The SiO_2 content of matrix glass-shards ranges from 68.5 to 71.6 wt.-% (EMPA; Table A3), which is significantly higher than the correlative ignimbrite whole-rock values (56.9–66.3 wt.-%; Tables A1 and A2).

Bulk pumice fragments in the crystal-poor units are of trachytic (Qasakh and Baghramyan) and dacitic (Amberd) composition (Fig. 3b; Tables A1 and A2); nevertheless, pumice matrix-glass within the bulk fiamme from older units show highly evolved subalkaline rhyolitic composition (SiO_2-content from 71.0 to 72.9 wt.-%). Within the Artik ignimbrite, the importance of magma mingling is emphasized by andesitic to trachyandesitic α-fiamme and (trachy-)dacitic to trachytic composition of β-fiamme (SiO_2-contents from 60.2 to 61.7 wt.-% and 63.6 to 66.0 wt.-%, respectively). In the Gyumri ignimbrite, the bulk fiamme show trachyandesitic composition (SiO_2-content from 62.2 to 62.3 wt.-%), reflecting a less evolved composition, whereas the bulk fiamme from the Shamiram-Byurakan ignimbrite show a wide range of SiO_2 composition ranging from 62.8 to 68.2 wt.-% (Fig. 3b; Tables A1 and A2).

In all analyzed AVP pyroclastic sheets, bulk pumice fragments and matrix glass of pumice, linear trends are revealed in some major element variation diagrams (Fig. 4a-d). MgO, TiO_2, and CaO display the negative correlation with SiO_2 (Fig. 3c-e), whereas K_2O shows a positive correlation with variable concentrations (1.7–5.3 wt.-%; Fig. 4d). Pumice and glass-shards in the older units (e.g. Qasakh) are products of more evolved MgO- and TiO_2-depleted melts (Fig. 3a, c; Table A3). Similar observations were made for the Gyumri, the youngest AVP pyroclastic unit. Exclusively, the bulk α-fiamme of Artik ignimbrite and its matrix glass are enriched in TiO_2 (Fig. 4c).

Other significant differences of AVP ignimbrites and associated pumice fragments can be seen in Sr and Zr vs. SiO_2 plots (Fig. 4e, f), which effectively discriminate between the Zr-rich older vs. Sr-rich younger units. The Zr content in the crystal-rich pyroclastic units and the associated pumice fragments is significantly lower (238–469 ppm) than in the crystal-poor ones (471–531 ppm; Fig. 4f). Assessing the composition of fiamme in the Artik unit, the highest Sr-content was observed in the α-fiamme (up to 509 ppm; Fig. 4e).

The primitive mantle-normalized variation diagram for immobile incompatible elements reveals pronounced negative Nb and Ta, Sr anomalies, and depletion in Ti and P, but positive Hf, Zr, Th, Rb, Ce and La anomalies for the AVP pyroclastic sheets and fiamme (Fig. 5a, b). It is remarkable that fiamme of the AVP ignimbrites are distinct from each other by their trace element (Sr, P, Zr, Hf, Y, Yb) composition (Fig. 5a, b). The pronounced negative Ti anomaly (Fig. 5a, b) and a high Nb/Ta ratio (up to 25; Table A1) suggest early fractionation of Fe—Ti oxides (Briqueu et al., 1984). The older ignimbrite units and fiamme are more depleted in P and Sr than the younger ones (Fig. 5b). This could be explained either by an early fractionation of apatite group minerals (Wilson, 1995), or by fractionation of early-formed An-rich plagioclase.

The AVP trachybasaltic and -andesitic lava display less enrichment in LREE compared to the pyroclastic units. The lava flows around the Aragats area (Tirin-Katar, Dashtaqar, Irind and Qasakh canyon) have

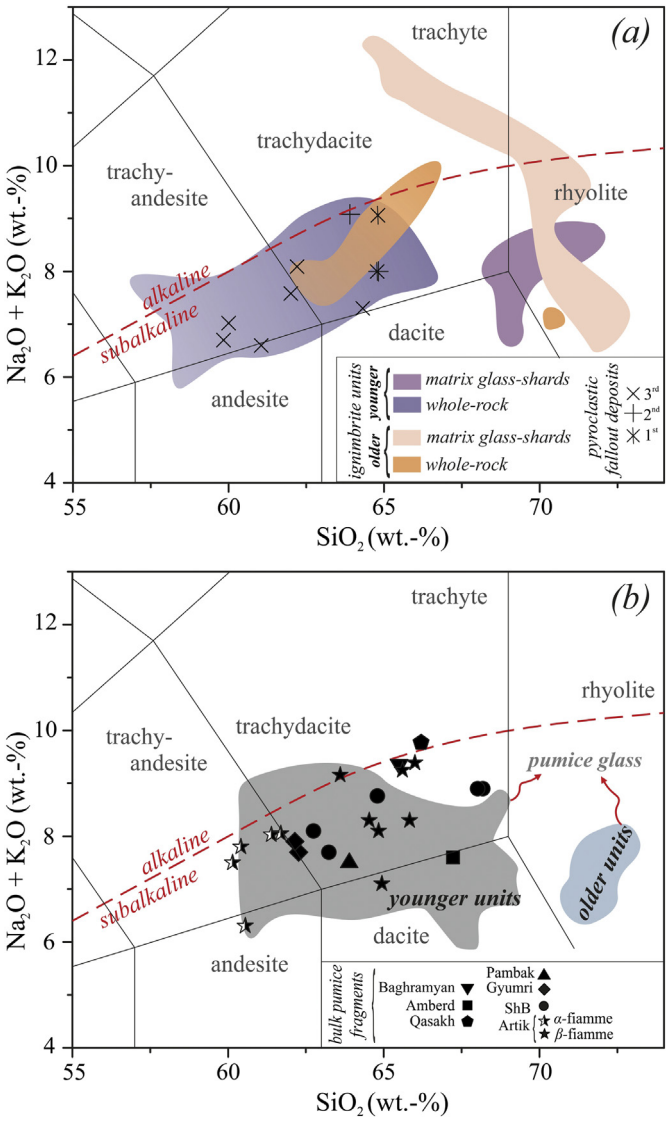

Fig. 3. TAS-diagrams of a) whole rock chemical composition of AVP ignimbrites and fallout deposits, and b) of associated pumice and glass shards: alkaline/sub-alkaline boundary after Irvine and Baragar (1971); ShB - Shamiram-Byurakan, (data in Tables A1, A2 and A3).

been considered by Meliksetian (2012) as representatives of the original trachybasaltic melt. Here, strong negative Nb—Ta, Sr, and Ti anomalies, and slightly positive Zr, Hf, Ce and La anomalies were observed (Fig. 5a, b; Meliksetian, 2012). The trachybasaltic and -andesitic lava of northern and central Armenia demonstrate similar signatures (Fig. 5a-d; Neill et al., 2015) as the ones from AVP lava flows.

The chondrite-normalized REE patterns of AVP pyroclastic sheets and related fiamme show a high LREE/HREE ratio (Fig. 5c, d). The different REE patterns support the split into younger and older ignimbrite units; the younger ones with higher LREE (La/Yb_{CN} = 12.3–14.4) and the older units with lower LREE (La/Yb_{CN} = 9.7–9.8). The weak negative Eu anomaly in the REE pattern of AVP pumice fragments (Fig. 5d) can be explained by feldspar growth in melts under moderate oxidation conditions, where Eu^{3+} cannot be incorporated into the plagioclase lattice (White et al., 2009).

4.3. Phenocryst textures and chemistry

4.3.1. Plagioclase

Plagioclase is the predominant felsic mineral (up ca. 50 vol.-% of the crystals population) in most of the AVP ignimbrites and it shows strong variation in textures and chemical composition ($An_{21.5}$ to $An_{49.8}$,

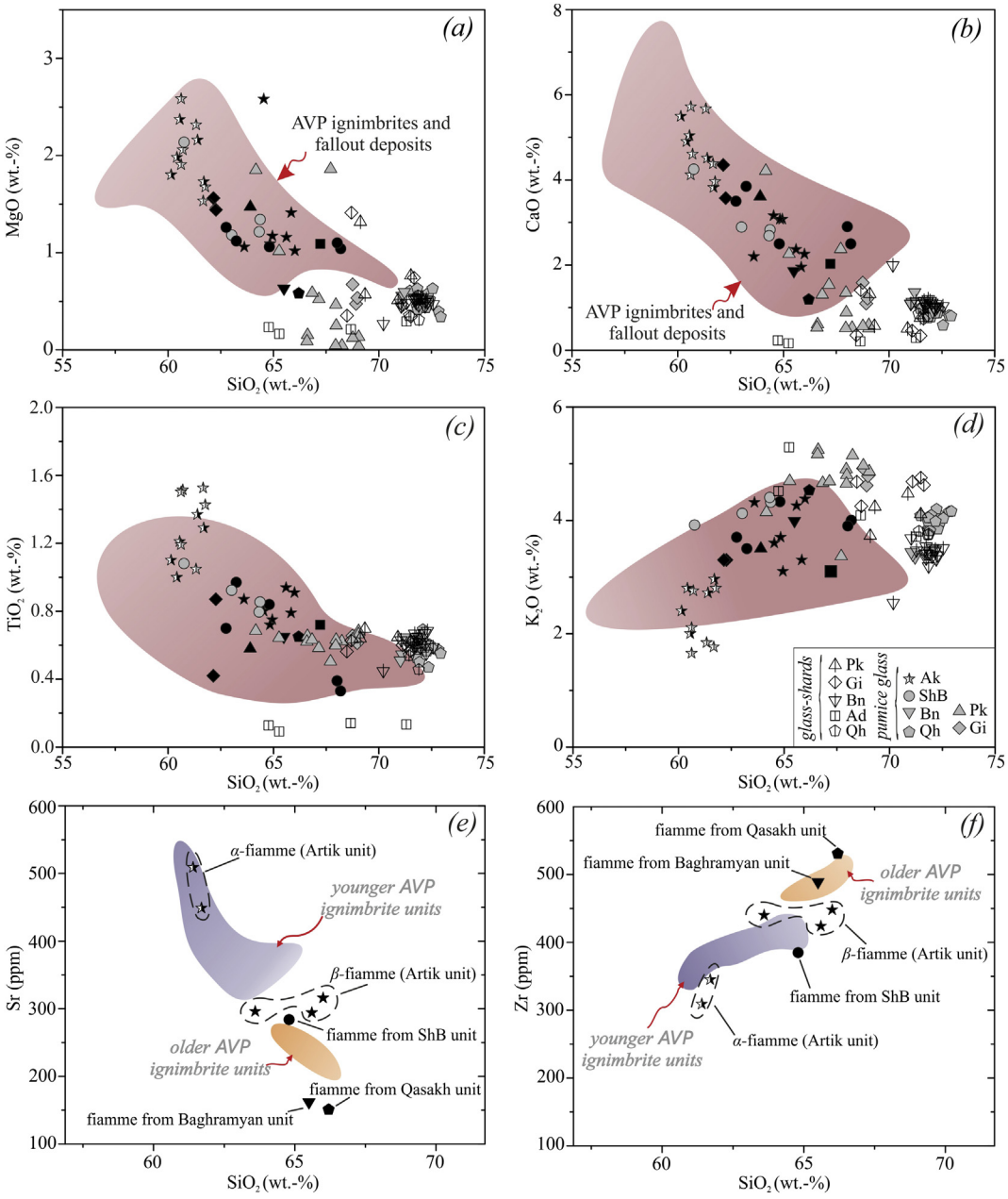

Fig. 4. Harker variation diagrams of selected major (MgO, CaO, K_2O, TiO_2) vs. SiO_2 for the AVP pyroclastic deposits and bulk fiamme, pumice glass and matrix glass-shards, e) Sr and f) Zr vs. SiO_2 for classification AVP ignimbrites and pumice fragments (bulk fiamme) within. For symbology see also Fig. 3 a, b; data in Tables A1, A2 and A3.

Table A4). It appears in euhedral to anhedral, tabular, needle- and lath-like shape as single grain or as an integral part of glomerocrysts. The largest specimen is in elongated tabular shape in the order of 2.0 to 5.5 mm (particularly in the younger units), whereas small needle- and lath-like plagioclase is restricted to sizes ranging from 100 to 700 μm. Most plagioclase of AVP ignimbrites shows similar ranges in chemical composition ($An_{26.4}$ $Ab_{65.7}$ $Or_{7.9}$ to $An_{49.8}$ $Ab_{47.4}$ $Or_{2.8}$) and textural style. However, in the older units, like Qasakh and Baghramyan, the composition is within a narrowly defined range ($An_{21.5}$ $Ab_{72.4}$ $Or_{6.1}$ to $An_{29.3}$ $Ab_{66.8}$ $Or_{3.9}$) and only a few specimens reveal resorption cavities filled by melt (glassy) material. High An-content (up to 56.9 mol.-%) can be reported for basaltic lithic fragments (Table A4; Fig. 6). Some glomerocrysts in the younger AVP units (e.g. Gyumri) show core compositions that are similar to those in plagioclase phenocrysts in the same thin section. The rim composition of the plagioclase phenocrysts is mainly identical to the composition of the groundmass microphenocrysts.

Particularly with plagioclase, phenocryst and glomerocryst texture displays external (coarse- and fine-sieve, dusty, spongy) and internal (normal, reverse, and oscillatory zoning) fabrics. In general, the degree of resorption increases from the oldest to the youngest units. Based on the combined textural and chemical analyses, at least three generations of plagioclase have been documented from the AVP ignimbrites: (1) the resorbed unzoned, (2) normal (Fig. 7a), reverse (Fig. 7b) or oscillatory (Fig. 7c) zoned and (3) euhedral unzoned. The first generation appears with moderate An-contents (up to 49.8 mol.-%; e.g. Gyumri and Shamiram-Byurakan units) and as An-poor variety (up to 29.3 mol.-%; e.g. Qasakh unit). The second generation displays normal zoning from An-rich core ($An_{48.0}$ $Ab_{49.2}$ $Or_{2.8}$) to An-poor rim ($An_{28.4}$ $Ab_{65.3}$ $Or_{6.3}$), few show reverse zoning from Ab-rich core ($Ab_{67.3}$ $An_{23.6}$ $Or_{9.1}$) to a relatively An-rich rim ($An_{48.9}$ $Ab_{48.3}$ $Or_{2.8}$). Oscillatory zoned plagioclase is commonly found in Artik ignimbrite, with An-poor core ($An_{27.7}$ $Ab_{67.0}$ $Or_{5.3}$) overgrown by a relatively An-rich mantle ($An_{46.6}$ $Ab_{50.7}$ $Or_{2.7}$) to again an An-poor rim. The third generation shows moderate

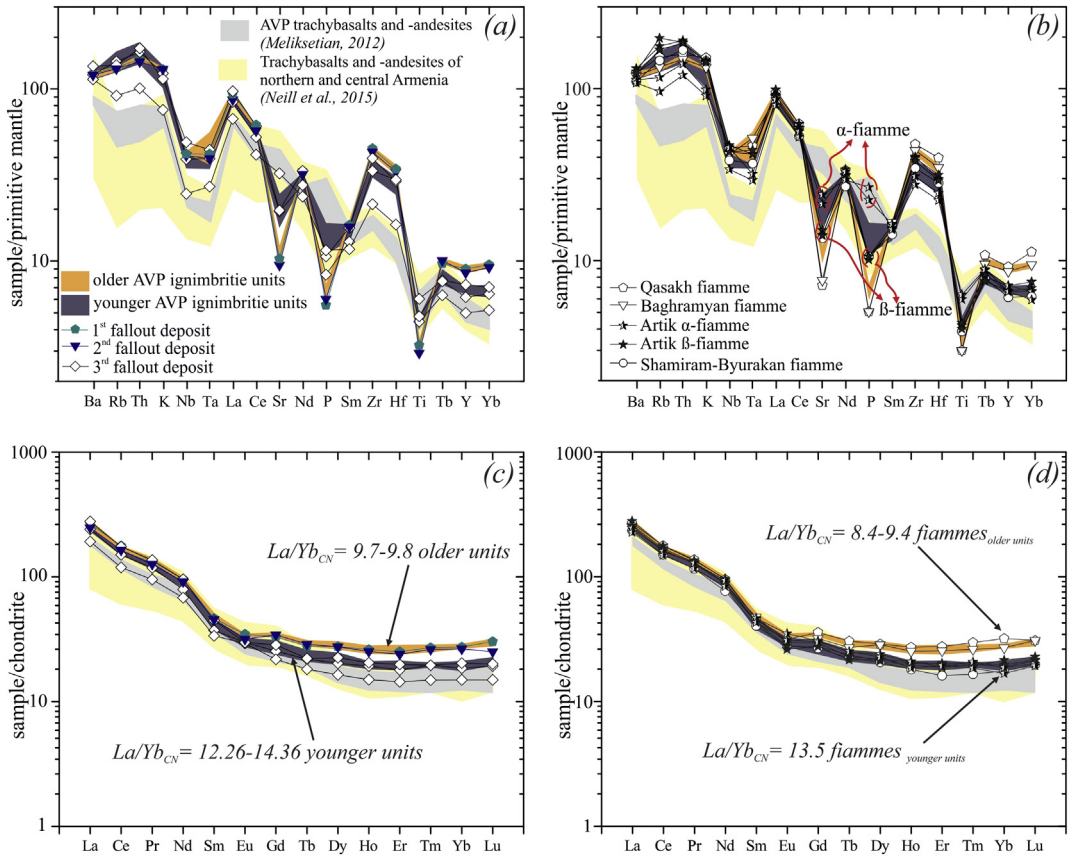

Fig. 5. a-b) Element variation diagrams of AVP ignimbrites and fallout deposits, and of AVP fiamme, normalized to primitive mantle (Sun and McDonough, 1989) and c-d) Chondrite-normalized REE patterns (Sun and McDonough, 1989) for the AVP ignimbrites and associated pyroclastic fallout deposits and pumice fragments (data in Table A1), Trachybasalts and –andesites of AVP (data from Meliksetian, 2012), northern and central Armenia (data from Neill et al., 2015).

An-contents in younger units (up to 47.6 mol.-%; e.g. Artik ignimbrite) and An-poor varieties (up to 28.4 mol.-%; e.g. Baghramyan ignimbrite) in older ones.

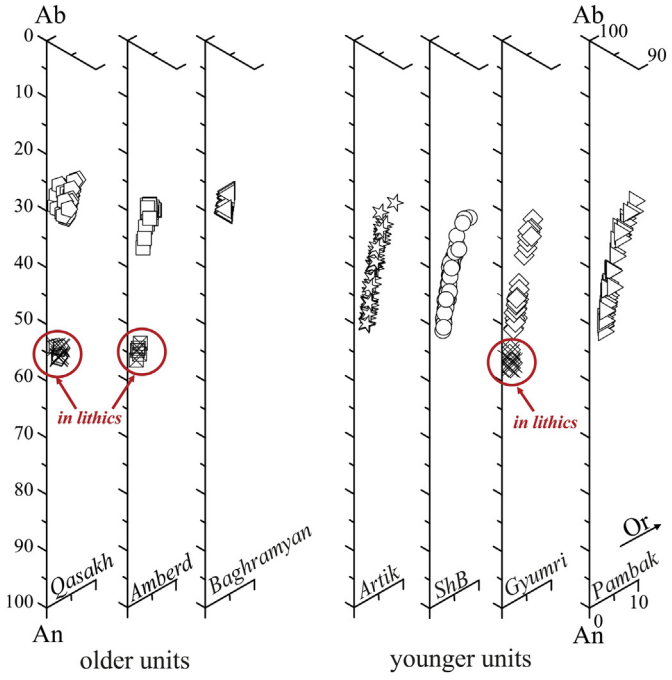

Fig. 6. An-Ab-Or ternary diagram showing composition of feldspar phenocrysts in AVP ignimbrites and basaltic lithics. Abbreviation: ShB - Shamiram-Byurakan (data in Table A4).

4.3.2. Pyroxene

Pyroxene is the most frequent ferromagnesian silicate (0.5 to 5.0 vol.-%) and is predominant in the younger pyroclastic units of Gyumri, Artik, and Shamiram-Byurakan. It mostly appears as part of glomerocrysts or as single grains in subhedral to anhedral shape, but also euhedral specimens can be observed. In general, grain size (0.1–2.6 mm) is smaller than the one in felsic silicate minerals. Few phenocrysts of ortho- and clinopyroxene show intergrowth textures and host inclusions of apatite. Most individual grains of clinopyroxene and orthopyroxene are chemically homogeneous with Mg# of 0.72–0.78 and 0.74–0.76, respectively. This clearly indicates growth of rims in more evolved melts. However, zoned pyroxenes have also been documented.

The quantitative analysis of orthopyroxene from the older ignimbrite units revealed Mg-rich enstatite ($En_{76.6}$ $Fs_{20.8}$ $Wo_{2.6}$) and Fe-rich enstatite ($En_{48.5}$ $Fs_{46.5}$ $Wo_{5.0}$, Fig. 8a). Clinopyroxene reveals higher Mg-contents with molar ratios of Mg_{82}:Fe_{18}, whereas orthopyroxene appears more ferrous (Mg_{73}:Fe_{27}). Within the Amberd ignimbrite, orthopyroxene shows change in composition from Fe-rich core to Mg-rich rim with Mg# of 0.51 and 0.76, respectively (Table A5; Fig. 8a). In the younger AVP units, clinopyroxene is predominant to orthopyroxene and it is represented by Ca-rich augite (up to 0.867 apfu; $En_{45.2}$ $Fs_{9.8}$ $Wo_{45.0}$) with high Mn-content. In contrast, clinopyroxene is very rare and more mafic in the older units with Mg # of 0.81–0.82 (Qasakh unit; Table A5) and most probably representing xenocrysts. Within the investigated samples, a weak zonation from Mg-rich cores to Fe-rich margins was observed in younger units. Additionally, few grains with reverse zonation can also be documented within the same sample. Solely, the Pambak ignimbrite additionally reveals diopside ($En_{44.6}$ $Fs_{9.3}$ $Wo_{46.1}$); its presence emphasizes the importance of high-Ca basaltic melt. Some grains show indications of early precipitation in more

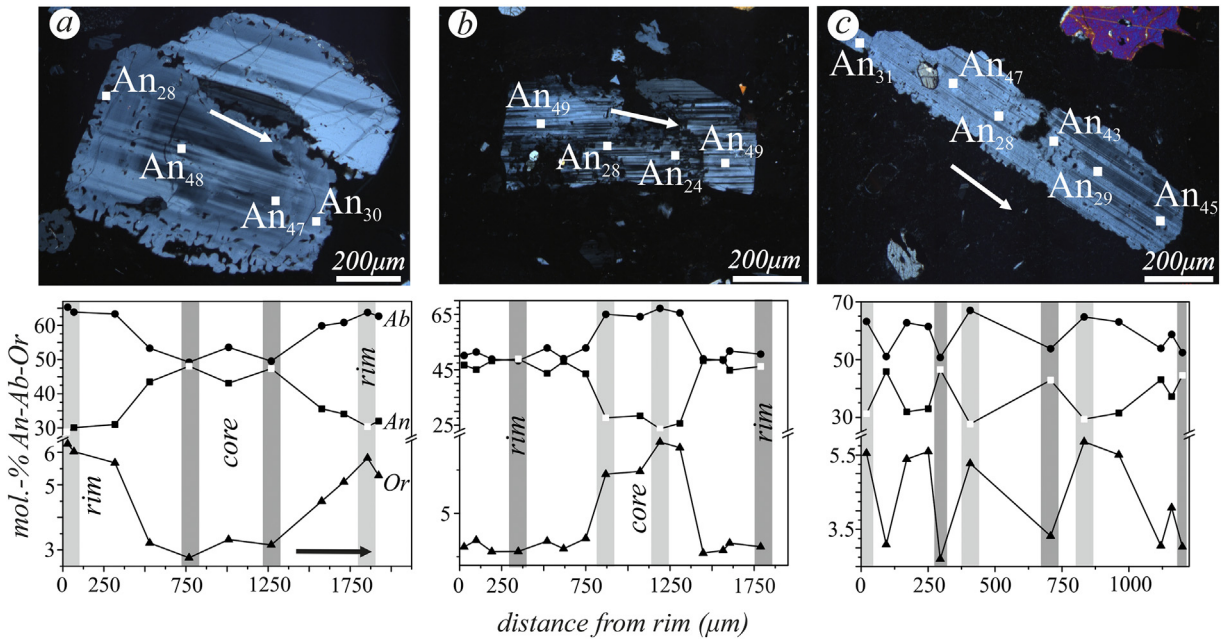

Fig. 7. Microphotographs (crossed nicols) and EPMA line measurements of a) normal (Ca-rich core and Na-rich rim) in Gyumri ignimbrite, b) reverse (Na-rich core and Ca-rich rim) in Pambak ignimbrite and c) oscillatory zoned plagioclase in Artik ignimbrite (data in Table A4): the arrow in the microphotographs indicates the profile line.

evolved melts as seen by the increase of Al and Si towards the crystal cores. Within the younger units, clinopyroxene shows remarkable concentration of Al_2O_3 and TiO_2 with contents up to 2.8 and 0.9 wt.-%, respectively. Hourglass sector zonation (Fig. 8b) appears in few grains of Artik ignimbrite. Formation of the hourglass texture depends on the substitution of $Al^{3+} \leftrightarrow Ti^{4+}$ at the M1 site (Nakamura, 1973; Welsch et al., 2016 and references therein). The dark-brown prism sectors are moderately enriched in Ti and Al (0.03 and 0.12 apfu, respectively), whereas the light yellow-brownish sectors are relatively enriched in Si (up to 1.96 apfu) and show lower Ti and Al concentrations (≤0.02 and 0.08 apfu, respectively). Some cumulates (Pl ± Cpx ± Opx ± Fe-Ti oxides) are partly resorbed. As a representative of early cumulates, clinopyroxene from AVP ignimbrites displays a compositional trend from subalkaline to tholeiitic, whereas clinopyroxene from AVP lava flows (data from Ghukasyan, 1983) shows compositional trend from subalkaline to tholeiitic and calc-alkaline (Le Bas, 1962; Fig. 8c, d).

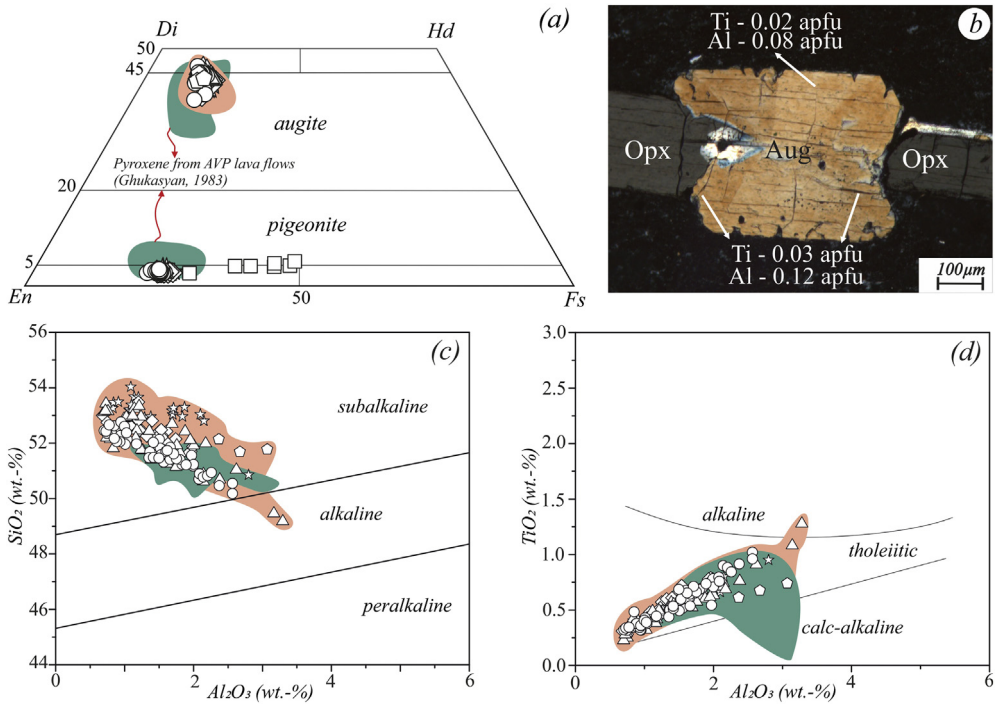

Fig. 8. a) Data of AVP pyroxene plotted in the classification diagram of Morimoto (1988); b) microphotograph of hourglass sector zoning in augite crystal (Artik ignimbrite); (c-d) bivariate discrimination diagrams of calcic clinopyroxene from AVP lava flows and ignimbrites (modified after Le Bas, 1962); for symbology see Fig. 6, data in Table A5.

4.3.3. Amphibole

All amphiboles are calcic with relatively constant CaO contents of 10.8 ± 0.4 wt.-% and are the most frequent (0.9 vol.-%) ferromagnesian silicates of the older AVP ignimbrite units (Qasakh, Amberd, and Baghramyan). They form euhedral-subhedral tabular crystals and appear as single grains and needle-like mineral fragments in the groundmass and as an integral part of the glomerocrysts together with plagioclase. The majority of the investigated amphiboles contain inclusions predominantly of apatite and Fe—Ti oxides. The chemical composition (calculated after Leake et al., 1997) reveals edinitic hornblende and magnesiohastingsite (Fig. 9a; Table A6), where Mg-contents range between 3.19 and 3.39 apfu. Within the lattice, the occupancy of alkalis (Na + K) at the A-site is of 0.63 to 0.70 apfu, with the occupancy of the B site, as follow: Na content ranges between 0.28 and 0.04 apfu and Ca content varies from 1.64 to 1.72 apfu. Regarding to the C and T positions, Ti content ranges between 0.14 and 0.40 apfu and Al^{IV} between 1.38 and 1.54 apfu (Table A6). The amphibole crystals from Qasakh and Baghramyan ignimbrites mainly have no reaction rims. However, some of the amphiboles reveal dehydration rims due to decompression, generated during magma ascent.

Few of the subrounded amphibole grains in Amberd ignimbrite are zoned and show clear reaction textures. Two amphibole reaction rims were distinguished within this unit based on texture, mineralogy, and thickness: (1) corona narrow/fine rim with 5.6 μm in width consists of breakdown products accompanied by needle-like plagioclase (up to 1 μm diameter) and Fe—Ti oxides with diameter from 1 to 2 μm (Fig. 9b). (2) Relatively coarse-grained titanomagnetite-bearing rims with up to 10 μm in width.

4.3.4. Accessory minerals

Accessory phases in the AVP ignimbrite units are represented by euhedral-subhedral Fe—Ti oxides and apatite. Fe—Ti oxide grains can reach 0.7 mm in size and occur as single grains, as an integral part of glomerocrysts, or they are present as inclusions in major phases. In terms of composition, the majority of studied magmatic minerals fall into magnetite-ulvöspinel (X_{mt} ranging from 0.57 to 0.93) and ilmenite-hematite solid solution series in the TiO_2-FeO-Fe_2O_3 system (Fig. A1). Single grains of ilmenite with X_{ilm} up to 0.86 (calculated after Carmichael, 1967) have been detected in AVP ignimbrites (Table A7). Trellis-sandwich type texture was detected in heterogeneous grains: lamellae of ilmenite of the host magnetite can be interpreted as a result of "oxidation-exsolution" or "oxyexolution" of former Ti-rich magnetite (Buddington and Lindsley, 1964; Haggerty, 1991). The formation of rutile is considered to be the final stage of primary Ti-rich magnetite/ilmenite decomposition (Fig. A1a-c). The occurrence and abundance of magnetic minerals in rocks are controlled by a variety of complex processes including magma composition and low-temperature oxidation of volcanic rocks (Nagata, 1961).

Apatite generally belongs to chlorapatite and hydroxyapatite with grain size up to 0.6 μm and it mainly occurs as inclusions in plagioclase, pyroxene, and amphibole in many AVP ignimbrites. Very rare micro crystals of zircon can be observed in the bulk matrix of almost all units, in some of the pumice fragments and in clinopyroxene phenocrysts (e.g. Gyumri ignimbrite).

4.4. Thermobarometry

The crystallization temperature and pressure were calculated based on the chemical composition of minerals and glass (EPMA) applying several thermo- and barometers (see Table A8). The matrix glass in AVP ignimbrite units represents the residual melt during the final stage of crystal growth. Thus, it is feasible to apply mineral-liquid thermobarometers such as the amphibole- (Molina et al., 2015; Putirka, 2016), plagioclase- and orthopyroxene-melt (Putirka, 2008). The equilibria between mineral and melt were determined by means of Fe/Mg relationships (Halama et al., 2006; Putirka, 2008, 2016; Rhodes et al., 1979). Additionally, sub-solidus systems were applied for thermometers in amphibole-only (Putirka, 2016), clinopyroxene-only (Nimis and Taylor, 2000; Putirka, 2008), amphibole-plagioclase (Holland and Blundy, 1990) and two-pyroxene (Putirka, 2008). All analyzed spots for the mineral-pair and mineral-melt systems are in equilibrium and in direct contact with each other.

The applied plagioclase-melt thermobarometers for glomerocrysts and for phenocrysts from the Baghramyan unit show a similar narrow range of crystallization temperatures between 1130 ± 33 and 1109 ± 27 °C. Whereas in the initial Qasakh unit, it resulted in significantly lower temperatures around 979 ± 87 and 994 ± 44 °C. The range of pressures for both units obtained is between 2.9 and 2.5 kbar (Putirka, 2008; Table A8).

Within the older AVP ignimbrite units, augitic clinopyroxene is mainly restricted to glomero- and phenocrysts of basaltic lithic fragments or it represents a xenocryst. The applied clinopyroxene-only thermobarometer (Putirka, 2008) shows similar crystallization temperature for clinopyroxene xenocryst 1281 ± 7 °C, and phenocryst from basaltic lithic 1287 ± 5 °C, with the high pressure up to 5.8 ± 0.5 kbar. Amphibole glomerocrysts show major changes in the crystallization temperatures in a range between 962 ± 4 °C (Qasakh ignimbrite) and 960 ± 7 °C (Amberd ignimbrite; amphibole-only, Putirka, 2016). These results are consistent with amphibole-plagioclase thermometry of Holland and Blundy (1990) under consideration of pressures estimated from amphibole-only barometry (Johnson and Rutherford, 1989). The calculated pressure obtained from the barometer of Johnson and Rutherford (1989) yielded in a range between 2.4 and

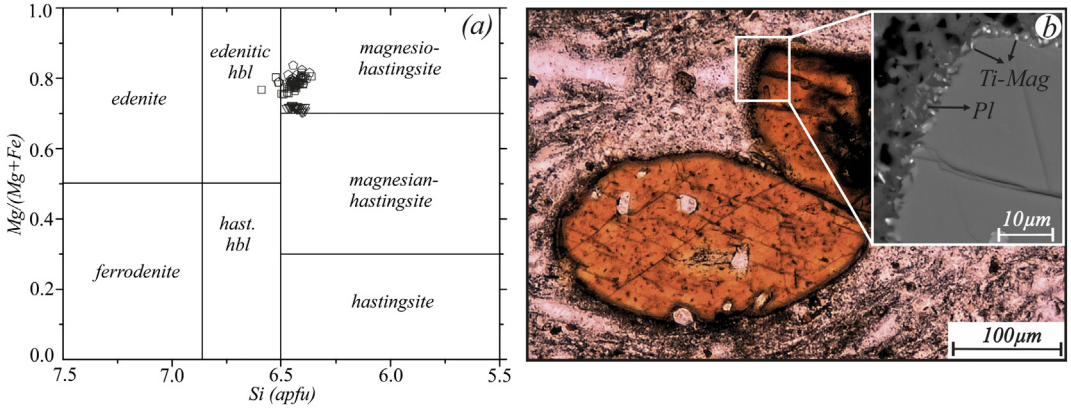

Fig. 9. a) Classification of amphibole from the Qasakh, Amberd and Baghramyan units plot in the Si (apfu) versus Mg/(Mg + Fe) diagram of Leake et al. (1997). For legend see Fig. 6. b) SEM-BSE image of breakdown rim of amphibole in Amberd ignimbrite (data in Table A6).

3.1 kbar with the maximum error of ±0.3 kbar. Assuming a crustal density of 2800 kg/m^3 (Kaban et al., 2016), this corresponds to an average depth of 11 ± 2 km. Amphibole-plagioclase thermometry yields temperatures in the range 958 ± 12 and 979 ± 8 °C, with little deviations, to the amphibole-only thermometer of Putirka (2016). In contrast the amphibole-melt thermobarometer shows the lowest crystallization temperatures in the range of 779 ± 32 to 729 ± 67 °C, Baghramyan and Qasakh unit, respectively (applying Putirka, 2016; Table A8).

The temperatures estimated by the clinopyroxene-only thermobarometer of Putirka (2008) show a nearly consistent range from 1266 ± 12 to 1285 ± 8 °C for the younger AVP ignimbrites. Here, temperatures above the basalt liquidus can be explained by relatively high crystallization pressure in the crust up to 5.3 ± 1.0 kbar. The subsolidus two-clinopyroxene thermobarometry (Putirka, 2008) indicates lower crystallization temperatures (up to 984 ± 16 °C for Gyumri ignimbrite). However, the orthopyroxene-melt thermobarometer yields the lowest crystallization temperature with 804 ± 4 °C for Gyumri unit (Putirka, 2008; Table A8).

5. Discussion

5.1. Re-evaluation of the AVP ignimbrites: Stratigraphy and textures

The stratigraphic column of the AVP ignimbrites has been re-evaluated based on direct field relations and their petrographic (phenocryst associations, textural characteristics, the degree of welding) and chemical characteristics (Fig. 2). As a result, the stratigraphic position of a few ignimbrite subunits and their correlation with well-known main units were re-allocated. Our fieldwork revealed Artik unit to be overlain by the Shamiram-Byurakan ignimbrite with a smooth transition. Furthermore, the distinction between Qasakh and Amberd units was established by means of petrological characteristics. In summary, based on areal extension, on correlation among flow units, and on petrographical and geochemical characteristics six stratigraphic units can be distinguished (from base to top): Qasakh, Amberd, Baghramyan, Artik, Shamiram-Byurakan and Gyumri (Pambak is stratigraphically equivalent to the Gyumri ignimbrite unit; Fig. 2).

In general, the AVP trachyandesitic-rhyolitic ignimbrites are characterized by a high degree of welding with eutaxitic to parataxitic texture. Together with a low lithic content (<5 vol.-%) they can be considered as 'high-grade' ignimbrites using the terminology of Walker (1983) and Branney and Kokelaar (1992). Ignimbrites with similar characters have been described from Gran Canaria (e.g. Schmincke and Swanson, 1967).

Based on variation in phenocryst and SiO_2 content, the AVP pyroclastic flow sheets can be divided into crystal-poor (Qasakh, Amberd, Baghramyan) and crystal-rich (Artik, Shamiram-Byurakan, Gyumri, Pambak) units (Fig. 10a). With the exception of Amberd unit (8 vol.-%), the AVP ignimbrite succession shows a general trend from low crystal content (e.g. Quasakh from 7 to 23 vol.-%) at the base to high crystal content towards the top. Gyumri unit reaches >40 vol.-% of phenocrysts.

Textural and whole rock/fiamme geochemical composition (Figs. 3–5, 10b) supports a co-genetic relation of the three documented fallout deposits with the respective overlying ignimbrites (e.g. "1st fallout unit" with Qasakh ignimbrite). These observations favor initial Plinian eruption with fallout followed by eruption column collapse resulting in deposition of ignimbrites for the three units: Qasakh, Bahgramyan, and Gyumri. Whereas, the lack of associated pyroclastic fallout deposits at the base of the Ambed, Artik, and Shamiram-Byurakan ignimbrites suggests formation from instantaneous collapse (Branney and Kokelaar, 2002).

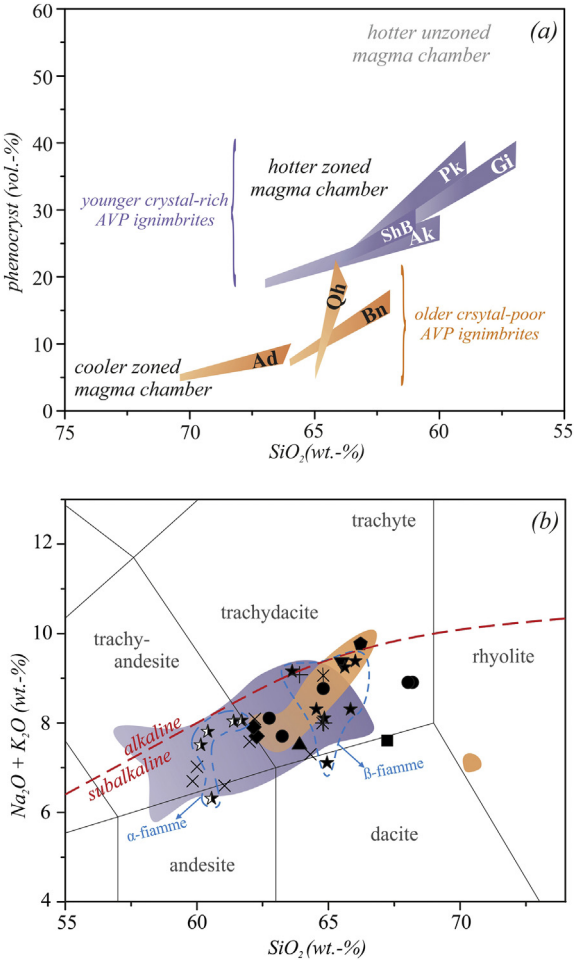

Fig. 10. a) The ignimbrite units of the Aragats Volcanic Province illustrated in the crystal-content versus SiO_2 diagram (modified after Hildreth, 1981). b) TAS-diagram of whole rock composition of AVP ignimbrites, associated fallout deposits and pumice fragments (alkaline/sub-alkaline boundary drawn after Irvine and Baragar, 1971). Abbreviations: Qh – Qasakh, Ad – Amberd, Bn – Baghramyan, Ak – Artik, ShB – Shamiram-Byurakan, Gi – Gyumri, Pk – Pambak. Symbols as in Fig. 3 a, b; data in Tables A1 and A2.

5.2. Melt evolution and affinities

The diversity of trace and major elements among the AVP pyroclastic sheets (e.g. 56–72 wt.-% SiO_2) can be attributed to the heterogeneity of the magma sources or, to such processes as crystal fractionation, assimilation, and magma mixing. Sparks et al. (1977) showed that a comparable compositional range (basaltic to dacitic/rhyolitic) may evolve due to injection of deeply-derived, volumetrically subordinate mafic melt into a shallow voluminous reservoir of rhyolitic magma.

The similar chemical composition of bulk pumice and fallout deposits (Figs. 3–5, 10b) suggests a co-genetic origin. Likewise, small compositional variation between the 1st, 2nd, and 3rd fallout deposits and their corresponding ignimbrites (Qasakh, Baghramyan, and Gyumri, respectively) indicates that each pair of deposits was generated from the same, geochemically homogenous magma chamber (Fig. 5a, c).

Pumice fragments are usually fresh in AVP ignimbrite units and therefore, their composition reflects the chemistry of the liquid part of the erupted magma. The major element composition of glass in pumice fragments shows that they are more Si-rich than bulk fiamme (Fig. 3b). The wide compositional range in fiamme from the Shamiram-Byurakan unit (SiO_2-content from 62.8 to 68.2 wt.-%; Figs. 3b and 10b) suggests an advanced mixing of melts, whereas the bimodal composition in fiamme (α- and β-fiamme) from the Artik unit indicates magma mingling (Figs. 3b, 4, 5b, d, and 10b; Tables A1 and A2). The bulk pumice

composition suggests that mingling and limited mixing occurred during or immediately before eruption. It is conceivable that the ignimbrite-forming eruption occurred in response to the injection of andesitic magma into a rhyodacitic magma chamber. The trend of enrichment in K_2O with increasing SiO_2 in both, pumice glass and ignimbrite glassy groundmass can be attributed to crystallization of groundmass minerals such as plagioclase, pyroxene, and Fe—Ti oxides (Harford et al., 2003). As the melt/glass-shard composition of the older units becomes more evolved (increase in K_2O), the plagioclase reveals more sodic composition.

Trace elements are usually decoupled from the major elements and show greater and more discriminative variation in volcanic glass. AVP rocks are characterized by enrichment in light rare earth elements LREE and large ion lithophile elements LILE (e.g., Ba, Rb and K), the latter, and flat HREE supports that garnet fractionation was not important. The aforesaid indicates partial melting of shallow upper mantle. This evidence has been also observed for the mafic rocks of northern and central Armenia (Neill et al., 2015). In addition, the AVP ignimbrites exhibit pronounced depletion in Nb, Ta and Ti and enrichment in K and Rb (Fig. 5a), which suggests an input of slab-derived fluids (e.g. Briqueu et al., 1984; Keskin et al., 1998; Pearce et al., 1990). The Zr/Nb vs. Zr plot (Fig. 11a) indicates significant levels of fractional crystallization. Given the high Rb/Th ratio typical for the continental crust, crustal assimilation was probably not significant in AVP (Fig. 11b; Pearce et al., 1990; Keskin et al., 1998). This statement is strongly supported by the limited variation in both the $^{87}Sr/^{86}Sr$ (0.704035 to 0.704414) and $^{143}Nd/^{144}Nd$ (0.512760 to 0.512863) isotope ratios obtained for almost all the AVP volcanic series, signifying the absence of substantial crustal assimilation at magma chamber levels beneath AVP (IAEA-TECDOC-1795, 2016).

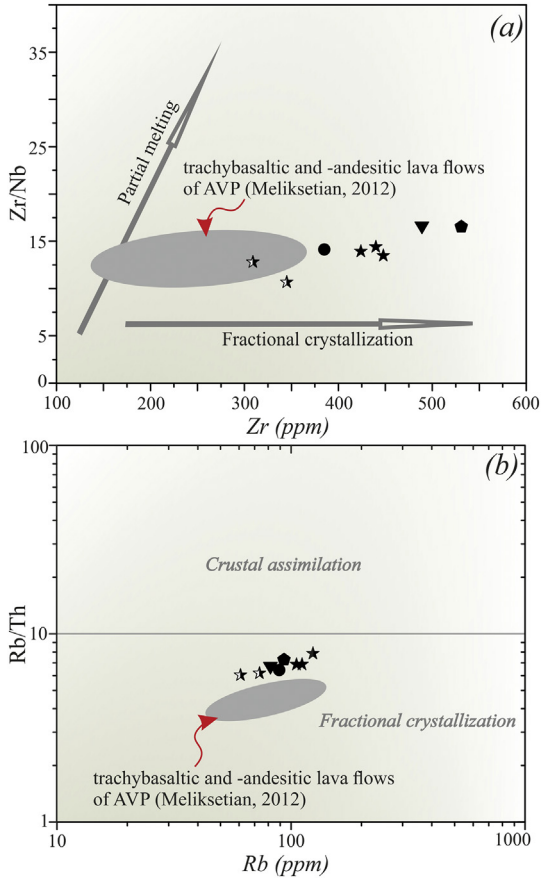

Fig. 11. Plots of a) Zr/Nb vs. Zr portraying the trends of partial melting and fractional crystallization, and b) Rb/Th vs. Rb illustrating the crustal assimilation and fractional crystallization for the analyzed samples from the pumice fragments of AVP ignimbrites. Vector arrows show the effect of increasing degrees of partial melting and fractionation. Symbols as in Fig. 3, data in Table A1.

High Zr (~ 300 ppm) content and Zr/Hf ratio (up to 43) have been observed in the mafic rocks of the whole Turkish-Iranian Plateau (Neill et al., 2015), which could suggest partial melting of enriched lithospheric mantle. Watson and Harrison (1983) assumed that Zr can only be incorporated in zircon. However, despite the high concentration of Zr (342–517 ppm; Table A1) in AVP pyroclastic units, the SEM-EDS and EMPA reveal only a few amounts of zircon within AVP ignimbrites, which can be due to several factors such as temperature and composition of the parent melt and lifetime in the magma chamber. High Zr content and high Zr/Hf ratios are also typical for Armenian post-collisional basaltic lavas (Neill et al., 2013, 2015). It was mentioned that basalts in north Armenia exhibit OIB like Zr (~200 ppm) concentrations and Zr/Hf ratios (47–52), this feature was attributed to mantle source characteristics and melting degree (Neill et al., 2013). If one assumes that trachydacitic melts of Aragats are fractionated from basaltic melt overprinted by magma mixing processes, then an accumulation of Zr in trachydacitic melts should result. Following Zhang and Xu (2016) there are several factors such as T (°C), H_2O and Zr concentration in the melt that can impact on the growth of zircon: (1) decreasing temperature is accompanied by diminishing of Zr diffusivity, and (2) in the same time increasing of H_2O is directly proportional to the increasing of the Zr diffusivity. It shows that zircon growth is much slower in rhyolitic melt and it also depends on the lifetime of the magma chamber. In this connection, we assume that the low concentration of zircon in matrix and pumice fragments within the AVP rhyolitic ignimbrites is the consequence of the short lifetime of the crystal-poor magma chamber. The increase in Zr content, going along with a decrease in crystal-content (Fig. 4f), could be linked to its incompatible behavior, which has also been observed in the Campanian ignimbrites (Forni et al., 2016 and references therein).

The AVP volcanic rocks formed in a post-collisional geodynamic setting; however, some geochemical characteristics of AVP rocks reveal a subduction fingerprint with negative Ta, Nb anomalies (Fig. 5a, b; see also Pearce et al., 1990). Also, a highly pronounced negative Eu anomaly, characteristic of plagioclase fractionation in many subduction settings, is lacking in the REE pattern of AVP ignimbrites (Fig. 5c, d). These results demonstrate a combination of subduction and within-plate geochemical characteristics, in good agreement with general evolutional tendency highlighted by Pearce et al. (1990) where collision-related volcanism is preceded by normal arc volcanism and followed by normal intraplate volcanism.

The pronounced negative Nb and Ta anomalies have been also observed for Neogene to Quaternary volcanic rocks of adjacent regions with a similar tectonic setting (e.g. Kars plateau in eastern Turkey, Pearce et al., 1990; Sabalan volcano in northwestern Iran, Shahbazi Shiran and Shafaii Moghadam, 2014). This geochemical signature is a typical characteristic of destructive plate boundaries (Pearce et al., 1990). However, these anomalies are also known from intra-plate volcanism and have been interpreted as either inherited fingerprint of underlying subduction-related rocks (e.g. Romer et al., 2001) or as result of a permanent crust-melt interaction of mantle-derived melts (e.g. Zegers and van Keken, 2001).

Subduction enrichment in the melt source region of the Quaternary volcanic sequences can also be detected in the Th/Yb vs. Ta/Yb and Th/Hf vs. Ta/Hf diagrams (Fig. 12a, b), where an “Arc-like character” can be observed. The characteristics of these evolved rocks may be generated by a number of processes, including melting of subduction-modified mantle sources, lower crustal melting, or assimilation of crustal materials with existing subduction-related geochemical signatures (Pearce, 1983). Trace element patterns of AVP pyroclastic fallout sheets and pumice fragments show a trend that is subparallel to the mantle array but shifted towards higher Th/Yb ratios. This feature indicates a lithospheric mantle source enriched by a subduction component.

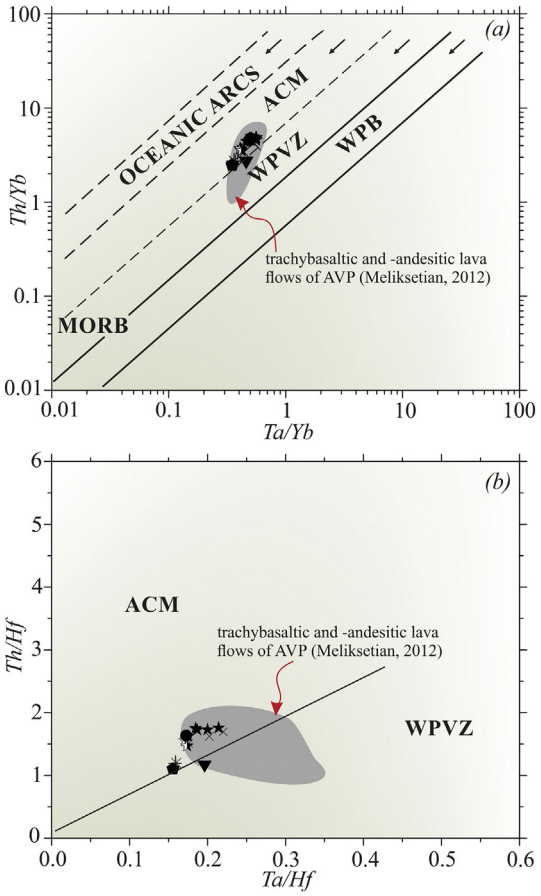

Fig. 12. Th/Yb vs Ta/Yb and Th/Hf vs Ta/Hf discrimination diagrams for AVP pyroclastic fallout sheets, pumice fragments and lava flows (Pearce, 1983; Schandle and Gorton, 2002; symbols as in Fig. 3a and b, data in Table A1). ACM = active continental margins; WPVZ = within plate volcanic zones; MORB = mid ocean ridge basalts; WPB = within plate basalts.

With AVP REE patterns, two trends are present (Fig. 5c, d). The older ignimbrite units tend to have elevated HREE, which could be attributed to the presence of amphibole as a mineral phase. The less enriched HREE of the younger ignimbrites can be explained by pyroxene-dominated fractionation.

5.3. p-T paths and magma dynamics

The mechanisms that lead to the formation of crystal-poor or -rich ignimbrites have been investigated by means of petrological and mineralogical studies (e.g. Ellis et al., 2014; Forni et al., 2016; Huber et al., 2012). Crystal-poor systems are known to be formed either in H_2O-rich zoned or hot "dry" unzoned magma chambers, whereas crystal-rich systems require mixing processes with the subsequent partial melting of the melt mush to erupt phenocryst-rich melt (e.g. Bachmann and Huber, 2016; Huber et al., 2012). These different dynamics in the magma reservoir can be tracked by the means of whole-rock geochemistry (e.g. Romer et al., 2001), mineral chemistry and textures (Crabtree and Lange, 2011; Renjith, 2014). Furthermore, petrographic observations, geochemical and microprobe analyses of coexisting melt inclusions and phenocryst assemblages can be used to determine equilibria or disequilibria in the magma prior to eruption (e.g., Halama et al., 2006; Rhodes et al., 1979). Internal and external zoning patterns of plagioclase phenocrysts and presence of different mafic mineral assemblages within AVP ignimbrites suggest that part of the mineral assemblage was in disequilibrium with the surrounding melt prior to eruption. The main evidence of disequilibrium between the surrounding melt and plagioclase in the younger AVP units is the existence of different textural sequence in plagioclase (normal, reverse zoned, highly resorbed and fresh grains) within a single thin section. The observed heterogeneity may have been developed by several factors: self-mixing, or multiple pulses of new crystal-rich magma from the deeper level (Couch et al., 2001), as well as magma mixing (Eichelberger, 1980; Tsuchiyama, 1985). Presumably, magma mixing resulted in overgrowths on once-resorbed phenocrysts and the nucleation of plagioclase microlites in the groundmass. In the remaining, unmixed portion of the felsic magma, some plagioclase underwent partial resorption but did not develop overgrowths.

In general, the degree of resorption increases from the older to the younger units displaying a relatively complete spectrum of plagioclase textures generating reverse zoning and resorption within the same unit. The analytical work of Ustunisik et al. (2014) explained that a decrease in pressure at constant temperature leads to the formation of reverse zonation in plagioclase. In contrast, isobaric crystallization results in normal zonation. Nevertheless, a common appearance of reverse and normal zonation is known as the consequence of magma mixing (Ginibre et al., 2007; Tepley et al., 2000). As common for mixing systems, more sodic plagioclase that formed in felsic magma component tends to be resorbed during injection of mafic melts into the magma chamber. Subsequently, the crystallization of more calcic plagioclase in the outer zones of phenocrysts took place. In this connection, experimental (Panjasawatwong et al., 1995) and analytical (Ustunisik et al., 2014) studies show that decompression leads to the formation of more An-rich rims (reverse zonation); contemporaneously, the phases of isobaric crystallization result in decreasing An-contents (normal zoning). This iterated changes of the crystallization conditions could yield in the formation of oscillatory zonation (Ginibre et al., 2007), which in turn indicates the convection-driven perturbation of the crystal in the melt (Renjith, 2014). The similar composition of the core of plagioclase phenocrysts and of glomerocrysts within the same sample (e.g. Gyumri, Artik units) can be interpreted in terms of growth in the same type of magma.

The highest degrees of resorption were observed within the younger AVP ignimbrite units (e.g. Gyumri), indicating a superheated magma chamber. Resorption cavities, fine and coarse sieve, and spongy texture can be reported for almost every plagioclase within the investigated samples. Likewise, few euhedral crystals show only marginal resorptions (fine sieve texture), which are known as the consequence of partial dissolution triggered by injection of Ca-rich melts (Renjith, 2014).

A common feature within the AVP ignimbrites is the appearance of coarse- and fine sieve textures that can be interpreted as either decompression and heating by recharging and superheating events or is the result of magma mixing (Blundy et al., 2006; Nelson and Montana, 1992; Tsuchiyama, 1985). The application of the plagioclase-melt geothermometry indicates increasing temperatures with decreasing SiO_2-content towards the top of the AVP pyroclastic sequence with a range of 979 to 1177 °C (Fig. 13a). With the obtained pressure of 2.6 to 4.5 kbar, it is inferred that crystallization environment was in the upper-middle crust of around 11 and 21 km depth for older and younger units, respectively (Figs. 13b and 15).

Basaltic injections into a superheated mushy magma body caused disequilibria between crystals and melt and favored the growth of "dry" ferromagnesian silicates like pyroxene. This is supported by the model of Huber et al. (2012) and Bachmann and Huber (2016), where crystal-rich intermediate pyroclastic rocks (e.g. Gyumri) are products of gradually zoned and hot magma chambers, while crystal-poor rhyolitic rocks (e.g. Amberd) were formed in cooler zoned magma chambers (Fig. 10a). The occurrences of amphibole- and pyroxene-bearing glomerocrysts suggest at least two generations of cumulate material, which are indicating different stages of crystallization in the Aragats magma reservoir. Amphiboles usually crystallize subsequent to pyroxenes in alkaline rocks. Their formation is related to an increase in the water content of the differentiating magma. The absence of reaction rims on amphibole crystals from Qasakh and Baghramyan ignimbrites can be linked to the fast ascent rate and high H_2O content in the

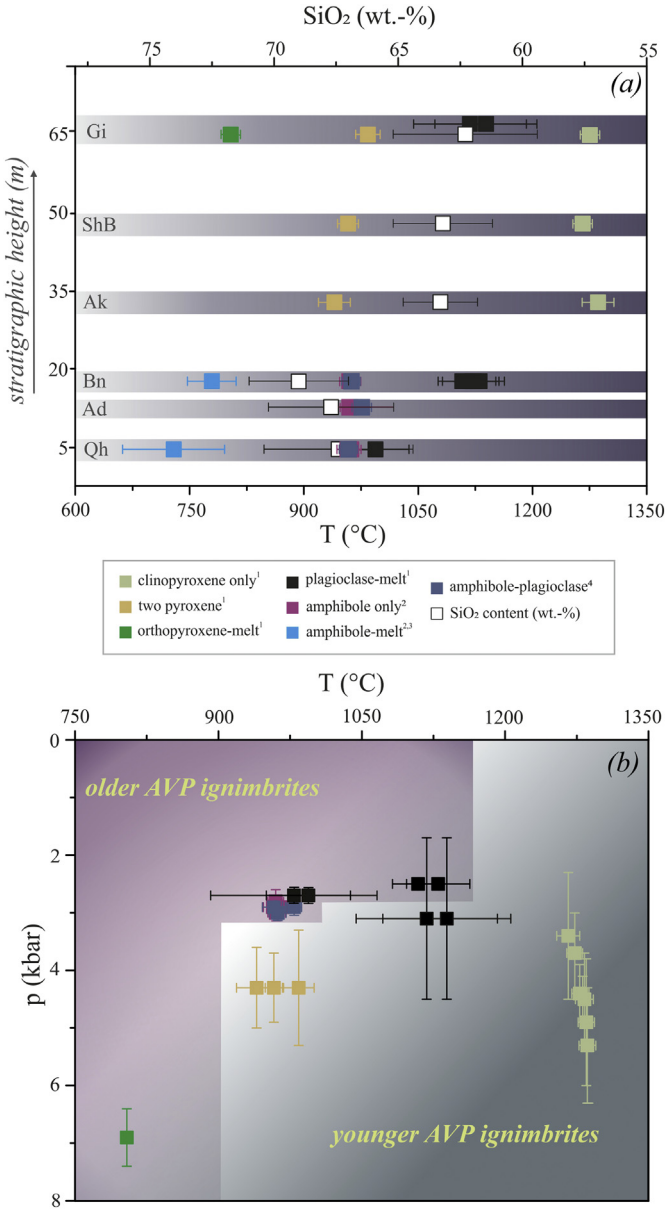

Fig. 13. a) Calculated T (°C) and SiO_2 content (wt.-%) for the different AVP ignimbrite units, b) p-T conditions of AVP magma reservoir: Applied thermometers and barometers, 1- Putirka, 2008; 2- Putirka, 2016, Johnson and Rutherford, 1989; 3- Molina et al., 2015; 4 – Holland and Blundy, 1990; Johnson and Rutherford, 1989 (see Table A8).

magma. AVP magnesiohastingsite and edinitic hornblende revealed fine-grained rims (5.6–10.0 μm) which are composed of microlites of Fe-Ti-oxides and plagioclase. These breakdown rim textures are known as products of rapid decompression where dissolution is minor (Nicholis and Rutherford, 2004). This means the rapid adiabatic ascent of the crystal and its surrounded melt causes the transition of magnesiohastingsite and edinitic hornblende into titanomagnetite and plagioclase (Browne and Gardner, 2006; Nicholis and Rutherford, 2004). Some 'microlites' are represented by fragments of amphibole, mechanically separated from the main phenocryst. Based on the studies of Rutherford and Hill (1993), these fine-grained bimodal microlite assemblages can only be formed in shallow magma chambers, which suggest rapid or multi-step decompression during magma ascent (Browne and Gardner, 2006; Nicholis and Rutherford, 2004; Rutherford and Hill, 1993). Whereas, coarse-grained breakdown rim with assemblages of orthopyroxene ± clinopyroxene + plagioclase + Fe-Ti-oxide can only be formed in deep-seated chambers. The reaction rims are texturally bimodal with respect to the size (maximum diameter) and shape (aspect ratio) of the crystals comprising them. The formation of coarse-grained Fe—Ti oxide bearing rim up to 10 μm in width can be interpreted as a result of single-step decompression during magma ascent from deeper crustal levels (Browne and Gardner, 2006; Rutherford and Hill, 1993).

Decompression experiments on Black Butte dacites (McCanta et al., 2007) and on compositionally similar dacites from Mount St. Helens (Rutherford and Hill, 1993) resulted in the interpretation of amphibole breakdown rim to be caused by decompression during magma ascent. The estimated crystallization temperature of AVP amphiboles (range of 703 to 971 °C, Fig. 13a) decreases with increasing silica content of the host melt, strongly suggesting the influence of magma composition on crystallization temperatures. Analyzed amphibole phenocrysts and glomerocrysts from the older AVP ignimbrite units generally yielded similar pressure estimates ranging between 2.4 and 3.1 kbar and thus indicating low-pressure fractionation (Rutherford and Hill, 1993). These pressure estimates and formation of narrow fine-grained breakdown rims of amphiboles in crystal-poor AVP ignimbrites imply the shallow nature of the magma chamber (Fig. 15).

Clinopyroxene is predominantly augite and minor diopside displaying a tholeiitic trend and suggesting that they resemble gabbroic cumulate fragments. The abundance of homogeneous phenocrysts of pyroxene in the AVP ignimbrites may indicate an equilibrium with the

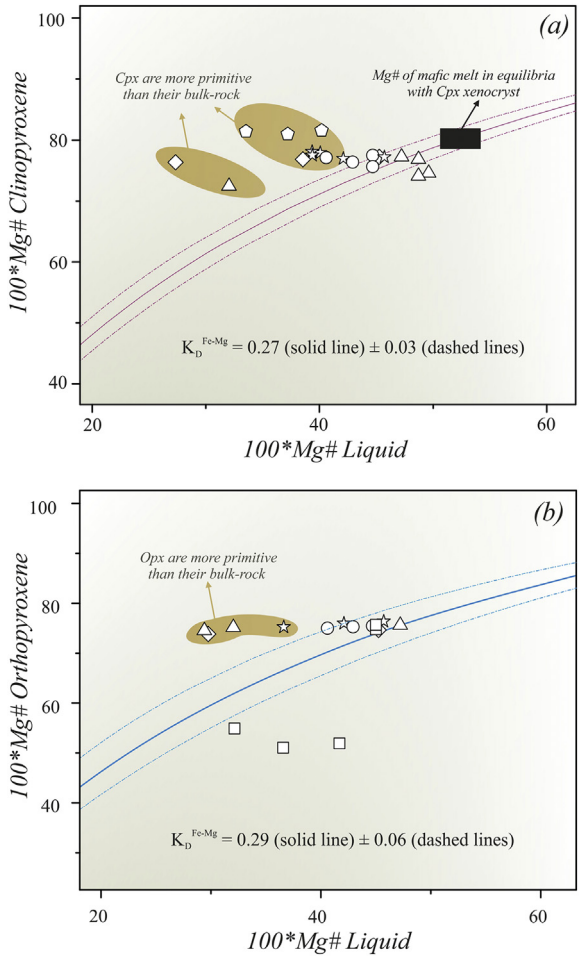

Fig. 14. Diagrams for equilibrium/disequilibrium condition, based on the Fe/Mg exchange reactions established by Rhodes et al. (1979), between a) clinopyroxene and liquid, and b) orthopyroxene and liquid. For the calculation of Mg# for pyroxene-melt equilibria, the bulk rock composition of AVP (trachy-) basalts, and basaltic trachyandesites (Mg# ~ 50–54) were taken from Ghukasyan (1983). Liquid = matrix glass-shards, symbols as in Fig. 6, data in Tables A3 and A5.

surrounding melt prior to eruption. However, contrasting Mg# of glass-shards of ignimbrite groundmass (27–49; Table A3) and of pyroxene phenocryst (51–78; Table A5) suggests that some of the pyroxenes were not in equilibrium with the melt (Fig. 14a, b). This supports the assumption of a hybrid nature of the AVP system, where mafic melts intruded resident silicic magma. It would also appear that formation of calcic clinopyroxene was influenced by injection of different types and portions of mantle melt into the magma chamber (Fig. 14a). The analyzed Mg-rich calcic clinopyroxene (Mg# up to 82) can be rather correlated to clinopyroxene of basaltic melts around the Aragats stratovolcano (Mg# ~79, Ghukasyan, 1983) than to the matrix glass-shards of the ignimbrite (Mg# up to 40). Thus, we interpret the studied clinopyroxene in Qasakh ignimbrite as xenocryst that originally crystallized in the basaltic melt (Fig. 14a). The Amberd orthopyroxene with a wide range of Mg# (51-core to 76-rim) initially crystallized in evolved magma and later have been re-mixed into more mafic magma (Fig. 14b).

The significant chemical variation found within the individual clinopyroxene crystals is reflected by hour-glass sector zoning (Artik ignimbrite), which can be interpreted as a result of rapid crystal growth where structural sites are in disequilibrium with the melt on different crystal faces (Nakamura, 1973). This discontinuous compositional trend across sectoral boundaries could also be triggered by rapid supercooling, which causes chemical disequilibrium during crystal growth (e.g. Welsch et al., 2016).

Pre-eruptive temperature and pressure values, estimated from the clinopyroxene geothermobarometer for the AVP ignimbrites, are in the range of 1253 to 1297 °C and 5.3 ± 1 kbar, respectively, supporting crystallization under moderate pressure in middle-crust magma chambers (Figs. 13, 14). Orthopyroxene comprises fresh phenocrysts of Mg-rich enstatite and crystallized in lower 804 ± 4 °C temperatures (Gyumri unit; Fig. 13a, b).

In summary, the mineral chemistry and -textures suggest non-uniform re-heating and remobilization of resident silicic magma by intrusions of hotter, mafic melts. Based on the assumed crustal density of 2800 kg/m^3 (Kaban et al., 2016) we presume the presence of an upper-crust reservoir at (~ 13 km depth) for amphibole-bearing magma and a deep-seated reservoir was tracked down to the depth around 25 km for amphibole-free/pyroxene-bearing magma (Fig. 15). Furthermore, converting the pressure estimates to the depth in conjunction with crystallization temperatures gives an opportunity to estimate an apparent geothermal gradient for the Aragats Volcanic Province in the time of volcanic activity. The obtained value of 7 to 9.5 °C per 100 m is higher than the estimated nowadays geothermal gradient of 5.5 °C per 100 m (Badalyan, 2000). Thus, using the latter gradient leads to overestimation of the depth of the AVP magma chamber.

In the aftermath of the Early Pleistocene high volume AVP explosive eruption of trachyandesitic to rhyolitic magmas, small batches of mafic melt ascended forming numerous isolated volcanic complexes at the flanks of Aragats. As the major and trace element geochemistry and the mineral chemistry revealed, all analyzed volcanic rocks from the Aragats Volcanic Province were originated from the same mantle source.

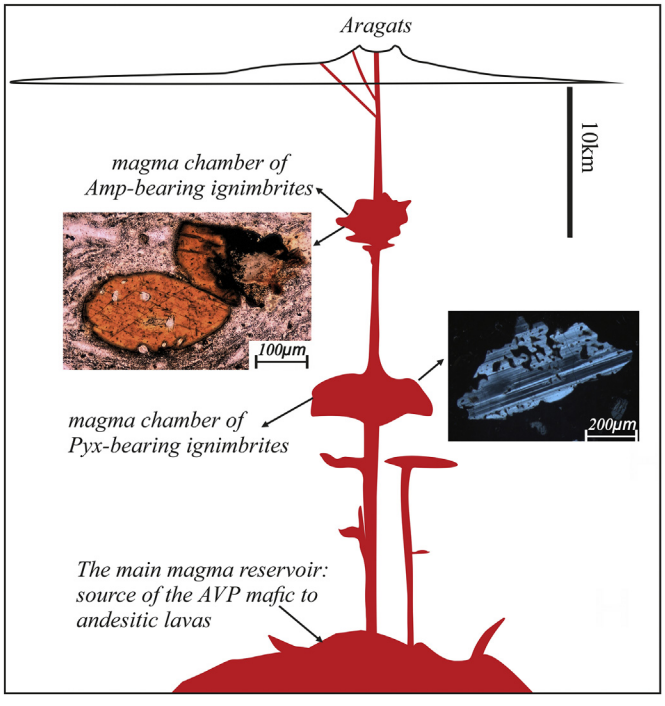

Fig. 15. Pre-eruptive schematic evolutionary model of the AVP-ignimbrite forming magma.

6. Conclusions

The Aragats Volcanic Province in western Armenia contains a comprehensive record of post-collision-related volcanism from ~2.50 to 0.45 Ma. Lava flows and pyroclastic deposits cover large areas with thicknesses up to 600 m or more. The principal conclusions based on field and petrological observations coupled with major and trace element analyses are summarized below:

(1) Re-evaluation of the Quaternary AVP pyroclastic flow sheets resulted in a distinction of six stratigraphic units representing distinct ignimbrite forming eruption episodes: Qasakh, Amberd, Baghramyan, Artik, Shamiram-Byurakan and Gyumri (including the Pambak ignimbrite).

(2) The textural and chemical observation on phenocrysts and bulk rock chemistry suggest two different levels of magma chambers: (i) cooler hydrous crystal-poor melts of upper crustal levels that generated the older ignimbrite units and (ii) hotter anhydrous crystal-rich melts of middle crust lead to the formation of the younger units. For the latter, magma mingling and mixing are confirmed by fiamme of different main and trace element composition.

(3) Application of numerous thermo- and barometers indicates at least two magma chambers, which were formed at depths around 10 to 13 km and ca. 25 km for the older amphibole-bearing and the younger amphibole-free units, respectively. With progressing volcanic activity, chamber(s) of successively deeper levels have been tapped during Plinian to Sub-Plinian eruptions.

(4) Geochemical data on bulk rock and fiamme allow for a clear distinction between the older and younger AVP ignimbrite units: high Zr- and Hf-contents, as well as low LREE/HREE ratios in the older units, can be attributed to crystallization of amphibole, whereas the younger units are dominated by crystallization of anhydrous minerals. Moreover, the heterogeneity of α- and β-fiamme within the Artik ignimbrite reveals that the re-equilibration of melt was not accomplished and the eruption of this ignimbrite occurred quickly upon remobilization.

(5) The Aragats stratovolcano evolved within an intraplate post-collisional tectonic setting. The presence of widespread younger basaltic lava flows, and textural and compositional evidence for magma mingling and mixing point to mantle-derived sources in the Aragats magma system. The geochemical model suggests fractional crystallization bear responsibility for the compositional diversity. Triggered by recurring recharge of mafic melts, the pre-eruptive mixing and mingling are the essential processes to remobilize portions of the crystal mush.

Supplementary data to this article can be found online at https://doi.org/10.1016/j.lithos.2018.07.024.

Acknowledgments

This work is dedicated to the late Dr. Alla Mnatsakanyan who contributed a lot in studying petrography and petrology of Armenian volcanism and made great efforts to teach young generation of volcanologists in the Institute of Geological Sciences of National Academy of Sciences of Republic of Armenia (IGS NAS RA). We gratefully acknowledge helpful discussions and support during fieldwork granted by R. Jrbashyan and Yu. Ghukasyan (IGS NAS RA). I. Neill (University of Glasgow, UK) is thanked for discussion on some of the ideas presented within. S. Gilbricht (TU Bergakademie Freiberg) is acknowledged for support of the work at SEM. We thank R. Halama (Keele University, UK) and an anonymous reviewer for their detailed and constructive comments and Xian-Hua Li for editorial handling. The study was funded in parts by the German Academic Exchange Service (DAAD) and by the U.S. Agency for International Development (USAID) through the U.S. National Academy of Sciences (NAS; PEER-Science Project 2-323, 2013-2016). Further support has been provided by the State Committee of Science of Republic of Armenia (grant #13-1E177, 2013-2015).

References

Bachmann, O., Huber, Ch., 2016. Silicic magma reservoirs in the Earth's crust. Am. Mineral. 101, 2377–2404.
Badalyan, M., 2000. Geothermal features of Armenia: a country update. Proceedings World Geotermal Congress, pp. 71–75.
Blundy, J., Cashman, K., Humhreys, M., 2006. Magma heating by decompression driven crystallization beneath andesite volcanoes. Nature 443, 76–80.
Branney, M.J., Kokelaar, P., 1992. A reappraisal of ignimbrite emplacement: progressive aggradation and changes from particulate to non-particulate flow during emplacement of high-grade ignimbrite. Bull. Volcanol. 54, 504–520.
Branney, M.J., Kokelaar, P., 2002. Pyroclastic Density Currents and the Sedimentation of Ignimbrites. Geological Society Memoir, London (152 pp).
Briqueu, L., Bougault, H., Joron, J.L., 1984. Quantification of Nb, Ta, Ti and V anomalies in magmas associated with subduction zones: petrogenetic implications. Earth Planet. Sci. Lett. 68, 297–308.
Browne, B.L., Gardner, J.E., 2006. The influence of magma ascent path on the texture, mineralogy, and formation of hornblende reaction rims. Earth Planet. Sci. Lett. 246, 161–176.
Buddington, A.F., Lindsley, D.H., 1964. Iron-titanium oxide minerals and synthetic equivalents. J. Petrol. 5 (2), 310–357.
Carmichael, I.S.E., 1967. The iron-titanium oxides of Salic volcanic rocks and their associated ferromagnesian silicates. Contrib. Mineral. Petrol. 14, 36–64.
Chernyshev, I.V., Lebedev, V.A., Arakelyants, M.M., Jrbashyan, R.T., Ghukasyan, Y.G., 2002. Geochronology of the Aragats volcanic centre, Armenia: evidence from K-Ar dating. Dokl. Earth Sci. 384, 393–398 (in Russian).
Couch, S.R., Sparks, S.J., Carroll, M.R., 2001. Mineral disequilibrium in lavas explained by convective self-mixing in open magma chambers. Nature 1037–1039.
Crabtree, S.M., Lange, R.A., 2011. Complex phenocryst textures and zoning patterns in Andesites and Dacites: evidence of degassing-induced rapid crystallization? J. Petrol. 52 (1), 3–38.
Djerbashyan, D.S., 2010. Petrology of lava flows of Aragats volcano. Armenian National Academy of Sciences, Gitutyun 131 pp (in Russian).
Eichelberger, J.C., 1980. Vesiculation of mafic magma during replenishment of silicic magma reservoir. Nature 288, 446–450.
Ellis, B.S., Bachmann, O., Wolff, J.A., 2014. Cumulate fragments in silicic ignimbrites: the case of the Snake River Plain. Geology 42, 431–434.
Forni, F., Bachmann, O., Mollo, S., De Astis, G., Gelman, S.E., Ellis, B.S., 2016. The origin of a zoned ignimbrite: insights into the Campanian ignimbrite magma chamber (Campi Flegrei, Italy). Earth Planet. Sci. Lett. 449, 256–271.
Gevorgyan, H., 2013. Genesis and stratigraphy of the Upper Pliocene-Quaternary tuff-ignimbrites of Armenia. Proceedings Young Scientist Conference, Institute of Geological Sciences, National Academy of Sciences of Armenia, Earth Sciences, pp. 18–27 (in Armenian).
Ghukasyan, Yu., 1983. Mineral-geochemical features of volcanic materials of Aragats Volcanic Province. Technical Report. IGS Academy of Sciences, Yerevan, Armenian SSR 355 pp (in Russian).
Ghukasyan, Yu., 1985. Petrography, Mineralogical-Geochemical Characteristics and the History of the Forming of Aragats Volcanic Complex. PhD dissertation. IGS Academy of Sciences, Yerevan, Armenian SSR 400 pp (in Russian).
Ginibre, C., Worner, G., Kronz, A., 2007. Crystal zoning as an archive for magma evolution. Elements 3, 261–266.
Haggerty, S.E., 1991. Oxide textures, a mini-atlas. Rev. Mineral. Geochem. 25, 129–219.
Halama, R., Boudon, G., Villemant, B., Joron, J.-L., Le Friant, A., Komorowski, J.-C., 2006. Pre-eruptive crystallization conditions of mafic and silicic magmas at the plat pays volcanic complex, Dominica (Lesser Antilles). J. Volcanol. Geotherm. Res. 153, 200–220.
Harford, C.L., Sparks, R.S.J., Fallick, A.E., 2003. Degassing at the Soufrière Hills volcano, Montserrat, recorded in matrix glass compositions. J. Petrol. 44, 1503–1523.
Hildreth, W., 1981. Gradients in silicic magma chambers: implications for lithospheric magmatism. J. Geophys. Res. 86 (B11), 10153–10192.
Holland, T.J.B., Blundy, J.D., 1990. Calcic amphibole equilibria and a new amphibole-plagioclase geothermometer. Contrib. Mineral. Petrol. 104 (2), 208–224.
Huber, C., Bachmann, O., Dufek, J., 2012. Crystal-poor versus crystal-rich ignimbrites: a competition between stirring and reactivation. Geology 40, 115–118.
IAEA-TECDOC-1795, Aspinall, W.P., Charbonnier, S., Connor, C.B., Connor, L.J.C., Costa, A., Courtland, L.M., Delgado Granados, H., Hibino, K., Hill, B.E., Komorowski, J.C., McNutt, S., Meliksetian, K., Nakada, S., Newhall, C., Samaddar, S.K., Savov, I.P., Self, S., Uchiyama, Y., Wilson, T., Yamamoto, T., 2016. Volcanic Hazard Assessment for Nuclear Installations: Methods and Examples in Site Evaluation (283 pp).
Irvine, T.N., Baragar, W.R.A., 1971. A guide to chemical classification of the common volcanic rocks. Can. J. Earth Sci. 8, 523–548.
Johnson, M.C., Rutherford, M.J., 1989. Experimental calibration of the aluminium-in-hornblende geobarometer with application to Long Valley caldera (California) volcanic rocks. Geology 17, 837–841.
Jrbashyan, R.T., Ghukasyan, Yu.G., Karapetyan, S.G., Mnatsakanyan, A.Kh., Navasardyan, G. Kh., Gevorgyan, H.P., 2012. The types of volcanic eruptions and the forms of manifestations of post-collision subaerial volcanism of Armenia. Arm. Natl. Acad. Sci. Inst. Geol. Sci. 3, 3–20 (in Russian).
Kaban, M.K., El Khrepy, S., Al-Arifi, N., Tesauro, M., Stolk, W., 2016. Three-dimensional density model of the upper mantle in the Middle East: interaction of diverse tectonic processes. J. Geophys. Res. 121 (7), 5349–5364.
Karakhanyan, A., Vernant, P., Doerflinger, E., Avagyan, A., Philip, H., Aslanyan, R., Champollion, C., Arakelyan, S., Collard, P., Baghdasaryan, H., Peyret, M., Davtyan, V., Calais, E., Masson, F., 2013. GPS constraints on continental deformation in the Armenian region and Lesser Caucasus. Tectonophysics 592, 39–45.
Karapetyan, K., 1992. The recent ignimbrite volcanism of the Republic of Armenia. Technical Report. IGS Academy of Sciences, Yerevan, Armenian SSR 550 pp (in Russian).
Keskin, M., Pearce, J.A., Mitchell, J.G., 1998. Volcano-stratigraphy and geochemistry of collision-related volcanism on the Erzurum-Kars plateau, northeastern Turkey. J. Volcanol. Geotherm. Res. 85, 355–404.
Koçyiğit, A., Yılmaz, A., Adamia, Sh., Kuloshvili, S., 2001. Neotectonics of East Anatolian plateau (Turkey) and Lesser Caucasus: implication for transition from thrusting to strike-slip faulting. Geodin. Acta 14, 177–195.
Le Bas, M.J., 1962. The role of aluminum in igneous clinopyroxene with relation to their parentage. Am. J. Sci. 260, 267–288.
Leake, B.E., Woolley, A.R., Birch, W.D., Burke, E.A.J., Ferraris, G., Grice, J.D., Hawthorne, F.C., Kisch, H.J., Krivovichev, V.G., Schumacher, J.C., Stephenson, N.C.N., Whittaker, E.J.W., 1997. Nomenclature of amphiboles: report of the subcommittee on amphiboles of the international mineralogical association, commission on new minerals and mineral names. Can. Mineral. 35, 219–246.
McCanta, M.C., Rutherford, M.J., Hammer, J.E., 2007. Pre-eruptive and syn-eruptive conditions in the black butte, California dacite: insight into crystallization kinetics in a silicic magma system. J. Volcanol. Geotherm. Res. 160, 263–284.
Melik-Adamyan, G.U., 1994. To the question of the upper bio-stratigraphic boundary of the Kasakh-Pambak type of ignimbrites of Armenia. NAS RA Earth Sci. XLVII (3), 9–12 (in Russian).
Meliksetian, Kh., 2012. Geochemistry of volcanic series of Aragats region. Natl. Acad. Sci. Inst. Geol. Sci. 3, 34–59 (in Russian).
Mitchell, J., Westaway, R., 1999. Chronology of Neogene and Quaternary uplift and magmatism in the Caucasus: constraints from K–Ar dating of volcanism in Armenia. Tectonophysics 304, 157–186.
Molina, J.F., Moreno, J.A., Castro, A., Rodriguez, C., Fershtater, G.B., 2015. Calcic amphibole thermobarometry in metamorphic and igneous rocks: new calibrations based on plagioclase/amphibole Al-Si partitioning and amphibole/liquid Mg partitioning. Lithos 232, 286–305.
Morimoto, N., 1988. Nomenclature of pyroxenes. Mineral. Petrol. 39, 55–76.
Nagata, T., 1961. Rock Magnetism. Maruzen, Tokyo (350 pp).
Nakamura, Y., 1973. Origin of sector-zoning of igneous clinopyroxenes. Am. Mineral. 58, 986–990.
Neill, I., Meliksetian, Kh., Allen, M.B., Navarsardyan, G., Karapetyan, S., 2013. Pliocene-Quaternary volcanic rocks of NW Armenia: magmatism and lithospheric dynamics within an active orogenic plateau. Lithos 180-181, 200–215.
Neill, I., Meliksetian, Kh., Allen, M.B., Navarsardyan, G., Kuiper, K., 2015. Petrogenesis of mafic collision zone magmatism: the Armenian sector of the Turkish–Iranian plateau. Chem. Geol. 403, 24–41.
Nelson, S.T., Montana, A., 1992. Sieve-textured plagioclase in volcanic rocks produced by rapid decompression. Am. Mineral. 77, 1242–1249.
Nicholis, M.G., Rutherford, M.J., 2004. 32 experimental constraints on magma ascent rate for the crater flat volcanic zone Hawaiite. Geology 32, 489–492.
Nimis, P., Taylor, W., 2000. Single clinopyroxene thermobarometry for garnet peridotites. Part I. Calibration and testing of a Cr-in-Cpx barometer and an enstatite-in-Cpx thermometer. Contrib. Miner. Petrol. 139 (5), 541–554.
Özdemir, O., Blundy, J., Güleç, N., 2011. The importance of fractional crystallization and magma mixing in controlling chemical differentiation at Suphan stratovolcano, eastern Anatolia, Turkey. Contrib. Mineral. Petrol. 162 (3), 573–597.
Panjasawatwong, Y., Danyushevsky, L., Crawford, A., Harris, K., 1995. An experimental study of the effects of melt composition on plagioclase-melt equilibria at 5-Kbar and 10-Kbar - implications for the origin of magmatic high - An plagioclase. Contrib. Mineral. Petrol. 118 (4), 420–432.
Pearce, J.A., 1983. Role of the sub-continental lithosphere in magma genesis at active continental margins. In: Hawkesworth, C.J., Norry, M.J. (Eds.), Continental Basalts and Mantle Xenoliths. Shiva, Natwich, pp. 230–249.
Pearce, J.A., Bender, J.F., De Long, S.E., Kidd, W.S.F., Low, P.J., Guner, Y., Saroglu, F., Yilmaz, Y., Moorbath, S., Mitchell, J.G., 1990. Genesis of collision volcanism in eastern Anatolia, Turkey. J. Volcanol. Geotherm. Res. 44, 189–229.

Peccerillo, A., Taylor, S.R., 1976. Geochemistry of Eocene calc-alkaline volcanic rocks from the Kastamonu area, northern Turkey. Contrib. Mineral. Petrol. 58, 63–81.
Peretyazhko, I.S., Savina, E.A., Karmanov, N.S., 2015. Comendites and pantellerites of Nemrut volcano, eastern Turkey: Genesis and relations between the trachyte-comenditic, comenditic, and pantelleritic melts. Petrology 23 (6), 576–622.
Putirka, K., 2008. Thermometers and barometers for volcanic systems. In: Putirka, K., Tepley, F. (Eds.), Minerals, Inclusions and Volcanic Processes. vol. 69. Reviews in Mineralogy and Geochemistry, pp. 61–120.
Putirka, K., 2016. Amphibole thermometers and barometers for igneous systems and some implications for eruption mechanisms of felsic magmas at arc volcanoes. Am. Mineral. 101 (4), 841–858.
Renjith, M.L., 2014. Micro-textures in plagioclase from 1994-1995 eruption, Barren Island Volcano: Evidence of dynamic magma plumbing system in the Andaman subduction zone. Geosci. Front. 6 (1), 113–126.
Rhodes, J.M., Dungan, M.A., Blanchard, D.P., Long, P.E., 1979. Magma mixing at mid-ocean ridges: evidence form basalts drilled near 22°N on the mid-Atlantic ridge. Tectonophysics 55, 35–61.
Ritchie, A.B.H., 1996. Volcanic Geology and Geochemistry of Waiotapu Ignimbrite, Taupo Volcanic Zone, New Zealand. Unpublished MSc thesis, University of Canterbury, Christchurch (153 pp).
Romer, R.L., Förster, H.J., Breitkreuz, C., 2001. Intracontinental extensional magmatism with a subduction fingerprint: the Late Carboniferous Halle volcanic complex (Germany). Contrib. Mineral. Petrol. 141 (2), 201–221.
Rutherford, M.J., Hill, P.M., 1993. Magma ascent rates from amphibole breakdown: an experimental study applied to the 1980–1986 Mount St. Helens eruptions. J. Geophys. Res. 98 (B11), 19667–19685.
Schandle, E.S., Gorton, M.P., 2002. Application of high field strength elements to discrimination tectonic setting in VMS environments. Econ. Geol. 79, 629–642.
Schmincke, H.U., Swanson, D.A., 1967. Laminar viscous flowage structures in ash-flow tuffs from Gran Canaria, Canary Islands. J. Geol. 75 (6), 641–664.
Shahbazi Shiran, H., Shafaii Moghadam, H., 2014. Geochemistry and petrogenesis of the Sabalan Plio-Quaternary volcanic rocks: implication for post-collisional magmatism. Iran. Soc. Crystallogr. Miner. 22, 57–68.
Shirinyan, K., 1961. Volcanic tuffs and tuffolavas of Armenia. Publishing House of the Armenian SSR Academy of Sciences, Yerevan 160 pp (in Russian).
Smith, R.L., 1979. Ash-flow magmatism. Geol. Soc. Am. Spec. Pap. 180, 5–27.
Sparks, R.S.J., Sigurdsson, H., Wilson, L., 1977. Magma mixing: a mechanism for triggering acid explosive eruptions. Nature 267, 315–318.
Steward, M.L., Pearce, T.H., 2004. Sieve-textured plagioclase in dacitic magma: interference imaging results. Am. Mineral. 89, 348–351.
Sun, S.-S., McDonough, W.F., 1989. Chemical and isotopic systematics of oceanic basalts: implications for mantle composition and processes. In: Saunders, A.D., Norry, M.J. (Eds.), Magmatism in the Ocean Basins. vol. 42. Geological Society of London Special Publication, pp. 313–345.
Tepley, F.J., Davidson, J.P., Tilling, R.I., Arth, J.G., 2000. Magma mixing, recharge and eruption histories recorded in plagioclase phenocrysts from El Chichón volcano, Mexico. Contrib. Mineral. Petrol. 41, 1397–1411.
Tsuchiyama, A., 1985. Dissolution kinetics of pagioclase in the melt of the system diopside-albite-anorthite and origin of dusty plagioclase in andesites. Contrib. Mineral. Petrol. 89, 1–16.
Ustunisik, G., Kilinc, A., Nielsen, R.L., 2014. New insights into the processes controlling compositional zoning in plagioclase. Lithos 200-201, 80–93.
Walker, G.P.L., 1983. Ignimbrite types and ignimbrite problems. J. Volcanol. Geotherm. Res. 17, 65–88.
Watson, E.B., Harrison, T.M., 1983. Zircon saturation revisited: temperature and composition effects in a variety of crustal magma types. Earth Planet. Sci. Lett. 64, 295–304.
Welsch, B., Hammer, J., Baronnet, A., Jacob, J., Hellebrand, E., Sinton, J., 2016. Clinopyroxene in post shield Haleakala ankaramite: 2. Texture, compositional zoning and supersaturation in the magma. Contrib. Mineral. Petrol. 171 (6), 1–19.
White, J.C., Parker, Don F., Ren, M., 2009. The origin of trachyte and pantellerite from Pantelleria, Italy: Insights from major element, trace element, and thermodynamic modelling. J. Volcanol. Geotherm. Res. 179 (1–2), 33–55.
Wilson, M., 1995. Igneous Petrogenesis - A Global Tectonic Approach. Chapman and Hall, London.
Zegers, T., van Keken, P.E., 2001. Middle Archean continent formation by crustal delamination. Geology 29, 1083–1086.
Zhang, Y., Xu, Z., 2016. Zircon saturation and Zr diffusion in rhyolitic melts, and zircon growth geospeedometer. Am. Mineral. 101 (6), 152–1267.